Chapter 6

COMPATIBILITY OF STRUCTURAL MATERIALS WITH LBE AND Pb: STANDARDISATION OF DATA, CORROSION MECHANISM AND RATE*

6.1 Introduction

The reasons for choosing lead (Pb) or lead-bismuth eutectic (LBE) as coolant and spallation target of accelerator-driven systems (ADS) have been mentioned in the introduction to this handbook. However, Pb and LBE show high aggressiveness for conventional structural materials. An understanding and mitigation of corrosion and degradation of mechanical properties of structural materials in Pb and LBE are essential issues for the demonstration of technical feasibility of critical and subcritical systems. In addition, the availability of technologies that allow for safe operation of lead alloy facilities is also essential.

Chapter 6 focuses on the compatibility of structural materials, mainly stainless steels, with lead-bismuth eutectic and lead, dealing with the corrosion mechanism and rate. First, the fundamentals of corrosion and protection methodologies by *in situ* oxide layer formation are discussed. Second, a critical review of the existing data on corrosion of structural steels in LBE and Pb is presented, with the main conclusions obtained from these data. Finally, recommendations on corrosion tests procedure are proposed.

6.2 Fundamentals

6.2.1 Corrosion

Structural materials exposed to liquid metals can undergo corrosion by: (1) direct dissolution of the solid metal in the liquid metal by a surface reaction involving atoms from the solid and the liquid metals or impurities present in the liquid metal, and (2) by intergranular attack. In the dissolution process or leaching, one component of the alloy is preferentially dissolved, as in the case of nickel that is leached from stainless steels by lead and lead bismuth eutectic [Sheir, 1994]. In the dissolution process two stages can be identified. The first stage involves "cleavage" of the bonds between atoms in the solid metal and the formation of new bonds with atoms of liquid metal or its impurities, in the boundary layer. Once this occurs, the dissolved atoms diffuse through the boundary layer into the liquid metal.

The driving force for corrosion is the difference between the chemical activities of the solute metals between the surface and the LBE. The chemical activity is dependent on the solubility and the chemical activity of the element in the solid phase, which is less than unity for all components in stainless steels. Therefore, the maximum concentration of the solute metal at the boundary of the two phases is determined by its chemical activity in the solid phase.

---

* *Chapter lead: Laura Soler Crespo (CIEMAT, Spain). For additional contributors, please see the List of Contributors included at the end of this work.*

The overall rate-controlling step is the diffusion through the boundary film of solute atoms into the flowing stream. Under static conditions at constant temperature:

$$a_i = a_o [1 - \exp(-\alpha St/V)] \quad (6.1)$$

where a_i is the concentration of solute after time t, a_o is the saturation concentration of solute in equilibrium with the solid state; S is the surface area of solid exposed to liquid of volume V, $\alpha = \alpha_o \exp[-\Delta E/RT]$, where E is the activation energy for dissolution.

Under isothermal and stagnant conditions, the laminar boundary is not as well defined as in a flowing system and the diffusion path cannot be defined.

The corrosion rate decreases with the time following an exponential law and the dissolution process stops when the concentration of the elements in the liquid metal reaches the saturation value. Therefore, corrosion by the direct dissolution process can be minimised by selecting a containment material whose elements have low solubility in the liquid metal of interest or by saturating the liquid metal before actual exposure. Measurements of weight changes as a function of time for a fixed a_o-a_i yield the kinetic information necessary for determination of the rate-controlling mechanism.

Under flowing conditions:

$$da_i/dt = K (S/V) (a_o - a_i) \quad (6.2)$$

where K is a rate constant, which is usually related to the diffusion rate through the boundary layer. In a flowing recirculating system, the precipitation process in the cold leg or heat removal part of the circuit often controls the steady-state concentration of the solute. The material dissolved at the highest temperature will precipitate at the lowest temperature until a steady state is reached. The corrosion rate is a function of both the maximum and minimum temperature in the circuit and the corrosion rate at the highest temperature can be reduced by increasing the minimum temperature or by reducing the maximum temperature [Weeks, 1997]. This type of corrosion is termed thermal gradient mass transfer. It can be illustrated by circulating a corrosive metal such as bismuth round a thermal convection loop of the type shown in Figure 6.2.1 [Weeks, 1956]. Mass is transferred from the hot zone to the cold zone and, after a period of time, the plugging of the loop may occur. This type of corrosion does not decrease with time, contrary to the observed in isothermal conditions. If the liquid metal is flowing at high velocity, the structural materials could be also subject to erosion-corrosion. The erosion can be classified to the widely damaged surface along the flow as if fluid carries out the surface material by a strong dynamic pressure and the pitting type erosion where material is deeply lost from narrow surfaces [Kondo, 2005].

Mass transfer can also occur under isothermal conditions where concentration gradients exist. The dissolved elements from one alloy can be transported by the liquid metal and precipitate or dissolve in another alloy, forming metal solid solutions or intermetallic compounds. In some cases selective dissolution can be used to advantage by “masking” one region of the system by material dissolved from another region of the system. Masking can be described as the lowering of element loss from a downstream region because a region rich in these elements is located upstream. For example, the removal of nickel from nickel containing alloys is an important factor determining the corrosion rate of these materials. If a high nickel source is placed upstream in an isothermal zone, the nickel removal rate from a region downstream could be reduced due to the higher Ni content in the coolant adjacent to this region which reduces the activity difference between the surface and the bulk.

Figure 6.2.1. Thermal gradient mass transfer [Weeks, 1956]

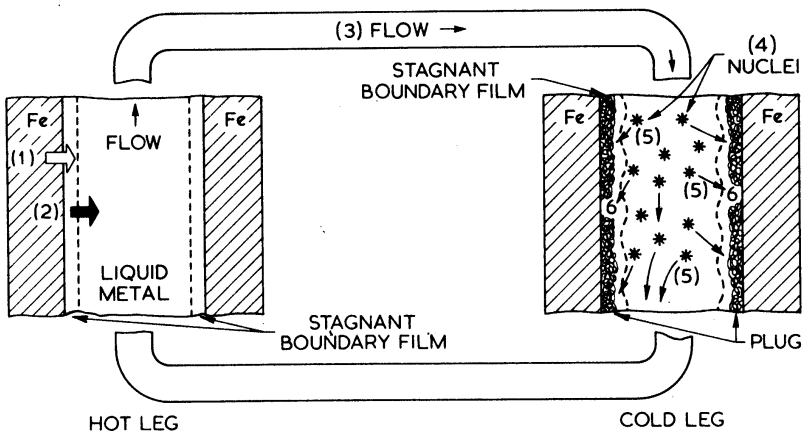

1. Solution
2. Diffusion
3. Transport of dissolved metal
4. Nucleation
5. Transport of crystallites
6. Crystal growth and sintering (plug formation)

Intergranular attack occurs because the atoms at the grain boundary have a higher potential energy than the atoms inside the grains. Therefore, the activation energy of the grain boundary atoms for dissolution is lower and the probability of their transition to the melt and, hence, the dissolution rate, higher. If the concentration of higher solubility elements increases in the grain boundaries, the dissolution rate may increase due to the preferential dissolution of these elements [Gerasimov, 1983].

A general discussion of the different types of corrosion in liquid metals and of the influence of several variables (temperature, temperature gradient, ratio metal solid area to liquid metal volume, velocity and others) can be found in [Staudhammer, 1992], [Bagnall, 1995].

6.2.2 Oxidation

Oxygen concentration in liquid lead alloys is a key parameter for the corrosion of structural materials. Several authors have correlated decreased dissolution resistance in Pb and LBE with low oxygen concentration. Gorynin, *et al.* [Gorynin, 1999] determined the influence of oxygen concentration on the corrosion/oxidation process of two austenitic stainless steels (18Cr-11Ni-3Mo commercial steel, and 15Cr-11Ni-3Si-MoNb experimental steel alloyed with 3% Si) in experiments performed in flowing lead at 550°C, for 3000 hours. For oxygen concentrations between 10^{-8} and 10^{-10} wt.%, corrosion by dissolution occurs whereas for concentrations higher than 10^{-7}-10^{-6} wt.% oxidation of steels takes place (Figure 6.2.2). The corrosion observed for low oxygen concentrations (10^{-8}–10^{-10} wt.%) begins with the formation of pits on the material surface. During exposure, the pits grow and merge into a porous corrosion layer, whose thickness grows linearly with time. Figure 6.2.2 shows the effect of oxygen concentration on corrosion resistance for stainless steels. There is a minimum in material loss associated with the formation of a protective oxide film.

Figure 6.2.2. Corrosion/oxidation of stainless steels in lead at 550°C [Gorynin, 1999]

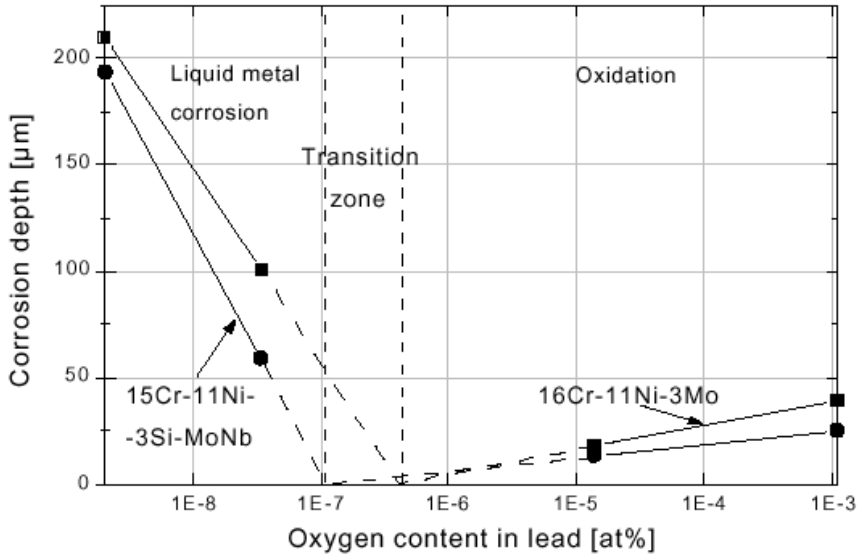

With an adequate control of the oxygen concentration in the liquid metal, the formation of oxide films on the surface of the structural materials occurs, limiting further dissolution. For the optimum effectiveness, the oxygen concentration in the liquid metal has to be adequate to passivate the material but not sufficiently high to promote the precipitation of lead oxide. For Fe containing alloys, such as structural steels, the minimum oxygen concentration is defined by the magnetite (Fe_3O_4) decomposition potential, considering this oxide the less stable of the ones that can be formed on structural steels. The maximum value is fixed by the precipitation of lead oxide. After the formation of oxide films, the dissolution of the structural materials becomes negligible due to the low diffusion rate of the alloying elements of steels in the oxides. The ideal protective oxide layer should be pore-free, crack-free, stress-free at operating temperatures, and resistant to spalling or damage during cooling or heating [Stott, 1987]. In addition, the oxygen and metal ions must have low diffusion coefficients through the scale and the recession rate of the original surface must be low enough during the desired service life [Kofstad, 1987]. For a practical lead-alloy coolant system, it is nearly impossible to set up such an ideal protective layer. However, it is possible to optimise the self-healing layer by controlling the oxygen concentration in the liquid lead/lead-bismuth, and changing steel compositions and operating conditions. This optimisation has finally the scope to minimise the corrosion-dissolution process and the corrosion-oxidation process.

Data on the influence of other elements on the corrosion resistance of structural steels in liquid lead alloys have been provided by Gorynin, *et al*. [Gorynin, 1998], [Gorynin, 1999]. For instance, Si increases the corrosion resistance of several steels in flowing lead-bismuth with oxygen concentrations lower than 10^{-7}wt.%, at 460°C, whereas for low oxygen concentrations (10^{-8}-10^{-10} wt.%) in lead at 550°C the Si influence is not significant [Gorynin, 1999]. The effect of other alloying elements such as Cr, Ti, Nb, Si and Al on low alloy steels corrosion in flowing lead-bismuth at 600°C was studied by the same authors. A significant decrease of the dissolution was observed for concentrations of Si and Al around 2% whereas for the rest of the elements, concentrations higher than 3% seem to be needed to obtain similar effects. In general, in reducing environments, in which the formation of protective oxide layers is not possible, steels with lower chromium concentration show lower dissolution rate. Austenitic steels suffer accelerated attack in lead and lead-bismuth due to the high nickel solubility. Yachmeniov has recommended limiting temperatures for the application of non-protected stainless steels to around 450°C for ferritic-martensitic steels and 400°C for austenitic steels [Yachmeniov, 1998].

The oxide layer structure of steel in liquid lead-alloys with oxygen control, in principle, depends on the steel composition, temperature and hydraulic factors. Generally, there are two possible oxide structures for martensitic steels according to the available experimental results [Balbaud-Celerier, 2003]:

- For temperatures below 550°C, it is composed of an external magnetite layer, Fe_3O_4 and a compact internal Fe-Cr spinel oxide layer. In some cases, the external magnetite layer is not observed. Penetrations of lead are sometimes observed in the outer layer. The duplex layer can protect steels from dissolution.
- For temperature above 550°C, an internal oxidation zone with oxide precipitates along the grain boundaries is observed below the Fe-Cr spinel layer.

Austenitic steels generally contain more Cr and Ni than martensitic steels. The oxide layer formed on austenitic steels has the following possible structures [Zhang, 2004]:

- For temperature below 500°C, the oxide layer is very thin and is composed of the single-layer Fe-Cr spinel, which can prevent direct dissolution.
- For temperature around 550°C, the oxide layer can have either duplex- or single-layer structure, depending on the surface and operating conditions. The duplex-layer oxide can prevent steel component dissolution, while heavy dissolution is observed when the single-layer oxide forms.
- For temperature above 550°C, heavy dissolution occurs.

For a static case, if the liquid is saturated with the steel components, no steel components can be further released to the solution. The oxide structures are then similar to that in gaseous environment. For other cases with scale removal, the possible oxide structures of stainless steels (martensitic or austenitic steels) in liquid lead-alloys with oxygen control are shown in Figure 6.2.3.

Figure 6.2.3. Possible oxide structures of stainless steels in liquid lead alloys with oxygen control [Chang, 1990]

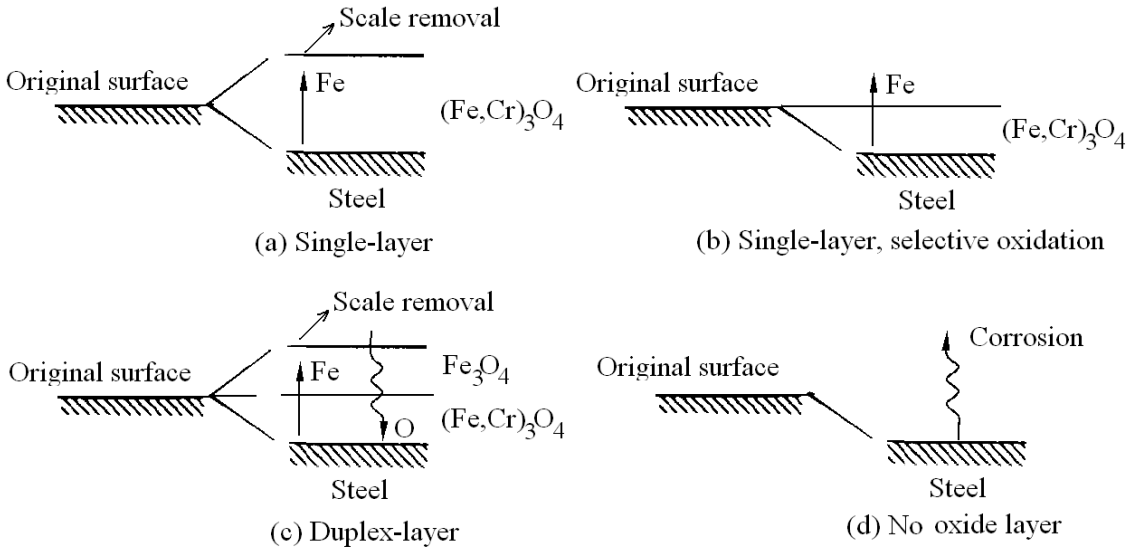

The oxide scale can be removed due to mass transfer corrosion. In practice, erosion can occur at locations where the flow changes its direction suddenly, such as a bend, an expansion, etc. The liquid particles can attack the protective layer and the high shear stress may strip the layer away. Such attacks can enhance the oxidation mechanism and lead to a higher degradation rate of the surface. Chang, *et al*. [Chang, 1990] classified the erosion-oxidation phenomena into four categories: 1) erosion of oxide only; 2) erosion enhanced oxidation; 3) oxidation affected erosion; 4) erosion of metal only. Rishel, *et al*. [Rishel, 1991] proposed that there are three types in erosion enhanced oxidation range (Figure 6.2.4).

Figure 6.2.4. Erosion-oxidation interaction regimes [Rishel, 1991]

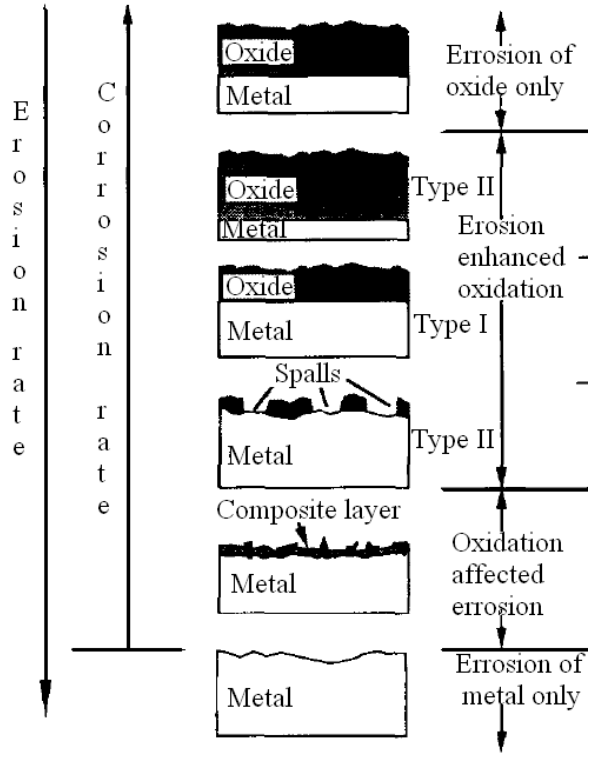

The active oxygen control technique is based on the fact that lead and bismuth are chemically less active than the major alloying elements of structural steels (Ni, Fe, Cr). The molar free energy of formation of the oxides of Ni, Fe and Cr is lower than that of lead and bismuth oxides, as can be seen in the Ellingham diagram in Figure 6.2.5.

To prevent PbO precipitation and to support Fe_3O_4 formation, the following conditions must be established:

$$2\,\Delta G^{o}_{PbO} > RT \ln p_{O2} > 0.5\,\Delta G^{o}_{Fe3O4} \qquad (6.3)$$

where ΔG^{o} is the Gibbs energy for formation of oxides, p_{O2} is the oxygen partial pressure, R is the gas constant and T is the absolute temperature.

Figure 6.2.5. Ellingham-Richardson diagram containing oxides of steel components and of Bi and Pb [Müller, 2003]

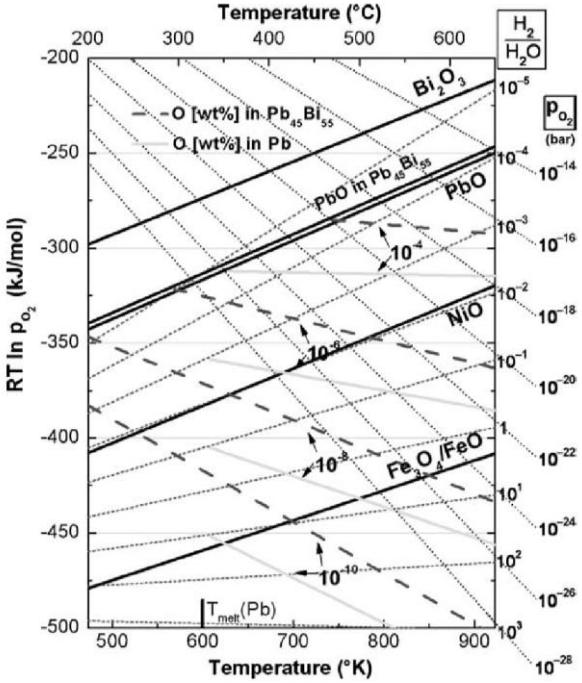

The reaction resulting in the formation/dissolution of magnetite in liquid lead or lead-bismuth can be expressed as:

$$4\ O + 3\ Fe \Leftrightarrow Fe_3O_4 \tag{6.4}$$

with the equilibrium constant:

$$Ke = a\ [Fe_3O_4]/a_o^4\ \ x\ a^3_{Fe} \tag{6.5}$$

where Fe, O and Fe_3O_4 are dissolved in the liquid metal, and a is the thermodynamic activity of the substances present in solution.

$$\text{If } a\ [Fe_3O_4] = 1 \Rightarrow a_o^4\ x\ a_{Fe}^3 = \text{constant at constant T} \tag{6.6}$$

For example, at 400°C and for $a_{Fe} = 1$, the equilibrium oxygen activity is 1×10^{-6} corresponding to an oxygen concentration of 1×10^{-10} wt.%. If $a_{Fe} < 1$, the oxygen activity will be higher.

The equilibrium oxygen activity as a function of the temperature for constant concentrations of oxygen and iron in lead-bismuth eutectic can be seen in Figure 6.2.6 [Li, 2002]. Steel corrosion via dissolution occurs below a minimum value of activity, $a_{min,}$ for which Fe_3O_4 is unstable, whereas coolant contamination by lead oxide formation takes places in the region above a = 1. Setting the maximum and minimum values of temperature of the liquid metal in a loop and assuming the oxygen concentration at minimum temperature equal to the saturation value, the permissible range of oxygen activity values can be determined.

According to Yachmenyov, *et al*. [Yachmenyov, 1998], an oxygen concentration $C_i > C_{min}$ will be necessary to form a protective film with the structure of spinel. C_{min} is the minimum concentration of

Figure 6.2.6. Equilibrium oxygen activity [Li, 2002]

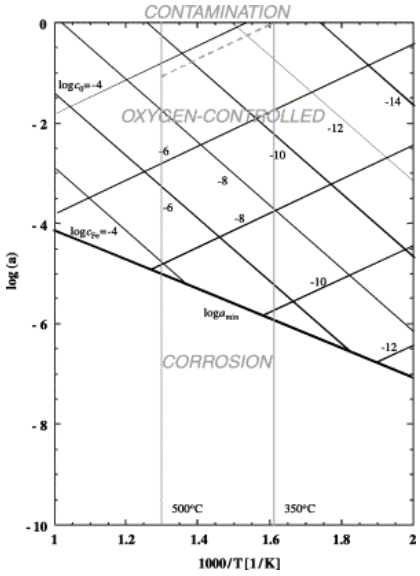

oxygen dissolved in the liquid LBE to maintain passivity of the materials. C_{min} must be higher than the equilibrium oxygen concentration for the magnetite existence, C^{T}_{min}, when $a_{Fe} = 1$. At $C_i < C_{min}$ substantial corrosion of the steels occurs. The morphology of corrosion depends on the value of $C = C_{min}-C_i$, but also on the steel composition, temperature and time. In practice, the corrosion process is kinetically controlled [Shamatko, 2000], and the corrosion of steels occurs for values of $C^{T}_{min} < Ci < C_{min}$ for which the process of steel dissolution prevails over that of steel oxidation.

During the system operation, different processes can modify the oxygen activity to values out of the permissible range. Impurities present in the coolant with oxides more stable than the iron oxide can decrease the oxygen concentration down to values lower than the needed for the formation of magnetite. Transmutation elements generated by the proton beam in the coolant can disturb the chemical equilibrium in the loop. Reduction-oxidation reactions can occur with the formation of non-soluble oxides, and with the reduction of the oxide protective layers [Gromov, 1998]. On the contrary, air in-leaks can increase the oxygen activity.

To control the oxygen activity in flowing liquid metal systems, several procedures have been developed in the past by Russian researchers [Efanov, 2001] and, at present, they are being revisited in different laboratories in Europe and USA [Knebel, 1999]. A detailed description of this procedure is given in Chapter 4 of this handbook, Section 4.3, entitled *Oxygen control in lead and LBE systems*. For oxygen control monitoring on line, electrochemical sensors for oxygen activity measurements were developed by Russian researchers and, recently, reference electrodes of In/In_2O_3, Bi/Bi_2O_3 and others are being developed and tested in several labs under different conditions. A detailed description of these sensors is given in Chapter 4, Section 4.4, *On-line electrochemical oxygen sensors*.

6.3 Summary and critical review of the data

The sources for the existing data on corrosion in LBE/Pb are the scientific literature on LBE and Pb technology, the TECLA European Project reports and international workshops on this subject. Corrosion tests of a wide variety of materials under wide ranging conditions have been carried out in both stagnant and flowing LBE/Pb. The steels tested include Fe-Cr steels, with chromium contents from 1.2 to 16.24 wt.% (SCM420, P22, F82H, STBA28, T91, NF616, ODS-M, Eurofer 97, STBA26,

Optifer Ivc, EM10, Manet II, 56T5, ODS, EP823, HT9, HCM12A, HCM12, 410ss, T410, 430ss). The composition of these steels is shown in Table 6.3.1. Austenitic steels tested include D9, 14Cr-16Ni-2Mo, 1.4970, 316L, 304L, and 1.4984. The composition of these materials are shown in Table 6.3.2. The test temperatures range from 300 to 650°C, times from 100 to 10000 hours and oxygen concentration in LBE/Pb from 10^{-12} wt.% to saturation. Tables 6.3.3-6.3.8 collect all the data available at each experimental condition. These tables are divided into: 1) Fe-Cr steels in stagnant LBE; 2) austenitic steels in stagnant LBE; 3) Fe-Cr steels in flowing LBE; 4) austenitic steels in flowing LBE; 5) steels in stagnant Pb; 6) steels in flowing Pb. Data included in the tables are the material, temperature, time, oxygen control system, oxygen concentration, exposed steel surface/LBE or Pb volume ratio and oxide layer thickness/dissolution depth or weight change measurement, and the reference. The general qualitative corrosion behaviour (oxidation or dissolution) is also included, following the indications of the authors. Some observations are also included concerning the morphology of the corroded steel surface. At least four different cases have been detected: 1) clear dissolution; 2) coexistence of relatively thin oxide layers with dissolution zones; 3) thick oxide layers, that, in some areas spall and in others allow the penetration of LBE; 4) clear oxidation. Of course, the two intermediate cases are difficult to interpret and a clear distinction is often not possible and subject to the author's interpretation. In Cases 1 and 2, dissolution is indicated and in Cases 3 and 4, oxidation. In the case of flowing conditions, the name of device (described in Chapter 12) and the fluid flow rate is included.

These tables collect all the data available. However, it is difficult to establish comparisons due to the wide range of experimental conditions used and the lack of standardisation of the corrosion tests. Not all the collected papers provided all the experimental conditions. In the cases in which oxygen contents are not reported, data have been considered invalid. This is the case of references [Soler, 2001], [Gnecco, 2004]. Other data have been included although the results were surprising, as it is the case of references [Benamati, 2002], [Long Bin, 2003], [Kurata, 2005], in which Manet martensitic steel and JPCA and 316ss austenitic steels tested at 550°C for 3000 hours present dissolution in oxygen saturated LBE. This data are marked with a star in Figures 6.3.1-6.3.10.

A first screening of the data was made using only the qualitative corrosion behaviour (oxidation or dissolution), eliminating the invalid data and using only the data of the longest duration tests, keeping the rest of conditions equal. With these data, a semi-quantitative analysis was made, representing the general corrosion behaviour in a graphic of temperature versus oxygen concentration. These graphics are shown in Figures 6.3.1-6.3.10. Specific graphics for the martensitic steel T91 and the austenitic steel AISI 316L are included, since these steels have been chosen as reference materials for further research in many laboratories.

In these graphics, the line of formation of magnetite and the saturation line (PbO formation) are indicated. Even though these graphics are semi quantitative (some points corresponds at different materials and times and only a qualitative indication of the corrosion behaviour is given), they are very useful to determine the temperature and oxygen concentration areas for which the protection by oxide layer formation is feasible. In all the cases, bellow the magnetite formation line dissolution takes place. In general, under stagnant LBE, at 600°C dissolution occurs and between 500 and 550°C there are dissolution or oxidation depending on the material. For austenitic steels, the general behaviour is similar, but the steels suffer stronger dissolution under reductive conditions and they present thinner oxide layers under oxidant atmospheres. In flowing conditions, there are less data, with a line around 10^{-6} wt.% oxygen concentration bellow which dissolution takes place. For T91 and 316L steels under stagnant conditions, there is dissolution at 600°C and bellow 10^{-6} wt.% oxygen concentration. Under flowing conditions, there are few data and the maximum temperature tested is 470°C, and it is not possible to get any conclusions. For steels tested in lead, there are very few data both under stagnant and flowing conditions.

Figure 6.3.1. Fe-Cr steels in stagnant LBE

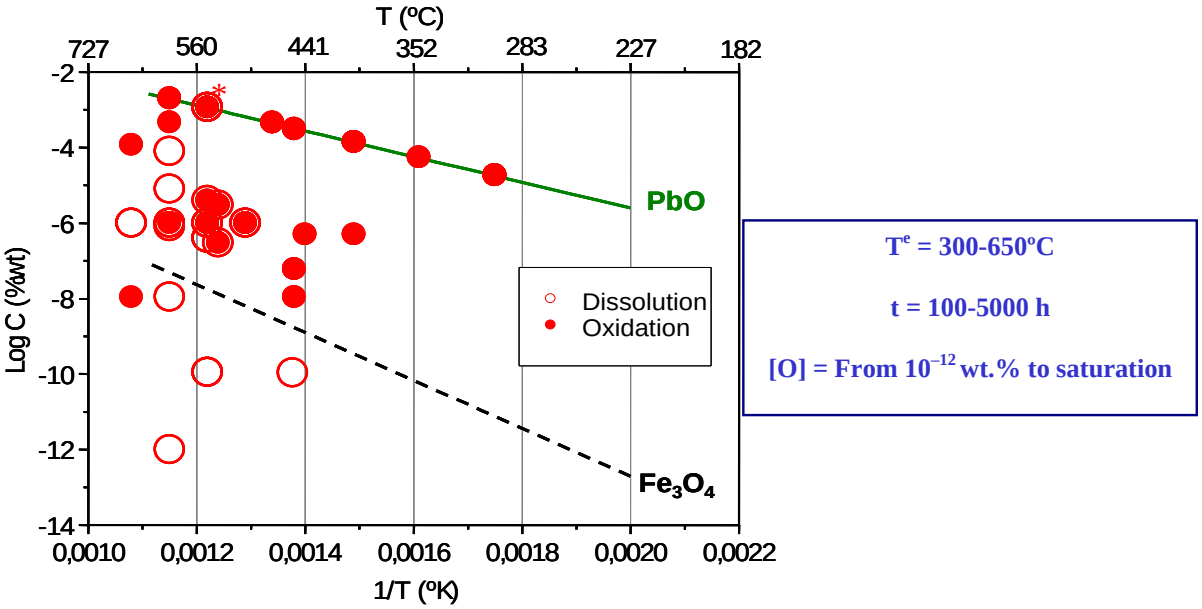

Figure 6.3.2. Fe-Cr-Ni steels in stagnant LBE

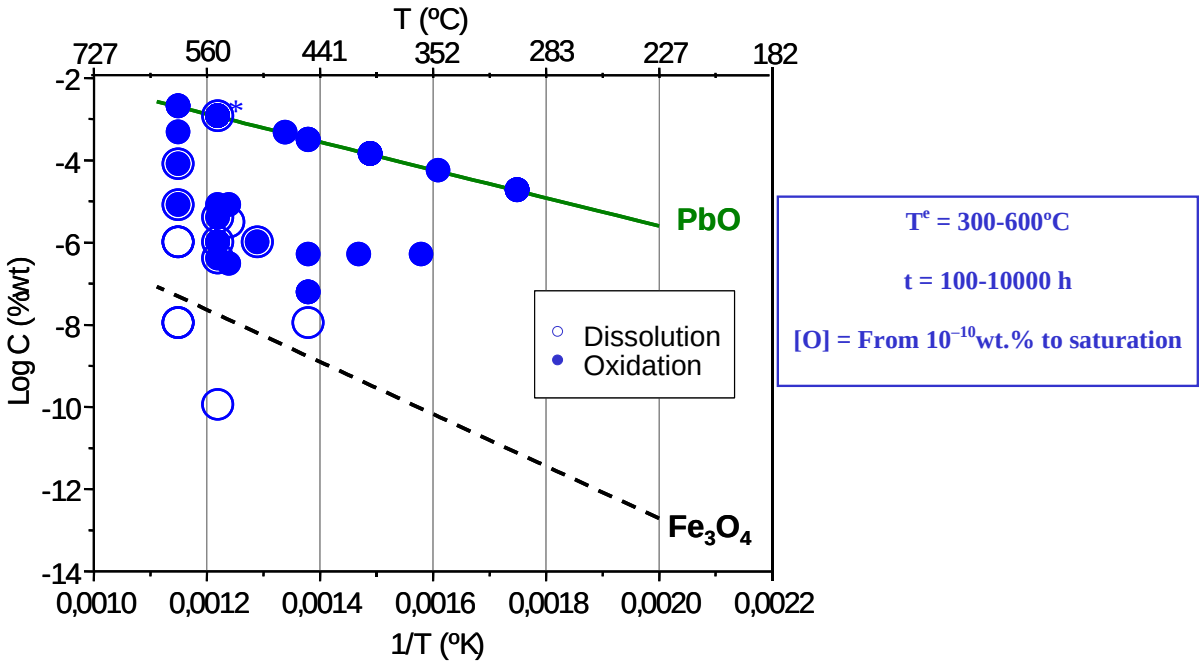

Figure 6.3.3. Fe-Cr steels in flowing LBE

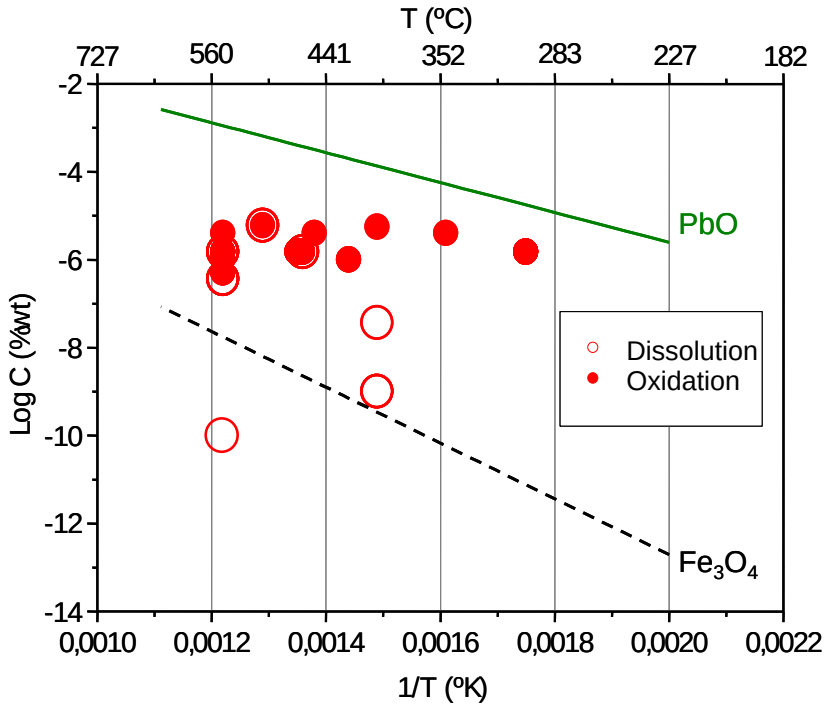

T^e = 300-600ºC

t = 340-7200 h

[O]= From 10^{-9} to 10^{-5}wt.%

Figure 6.3.4. Fe-Cr-Ni steels in flowing LBE

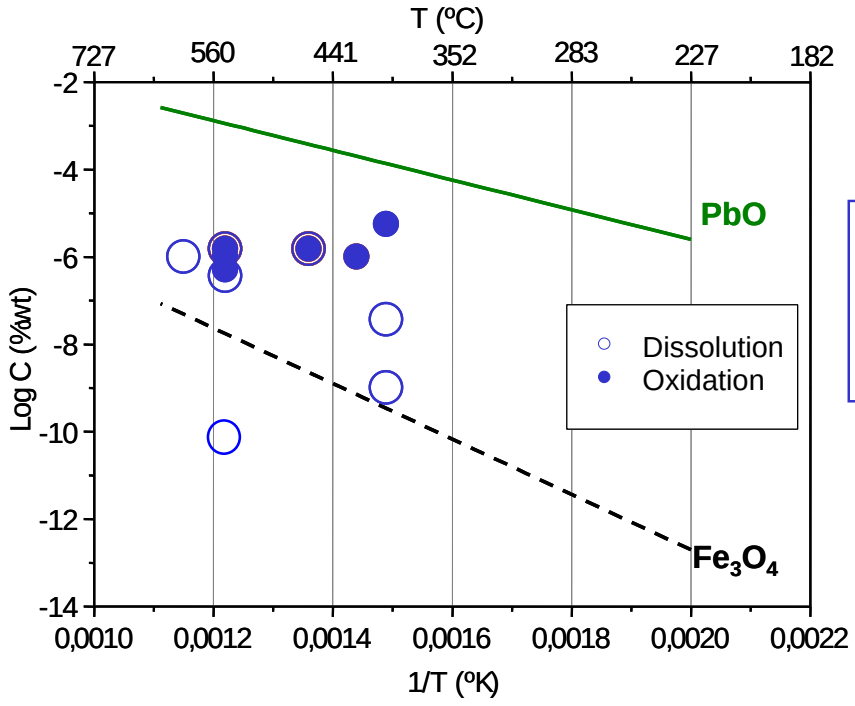

T^e = 400-600ºC

t = 700-7200 h

[O] = 10^{-9}-10^{-5} wt.%

Figure 6.3.5. T91 steel in stagnant LBE

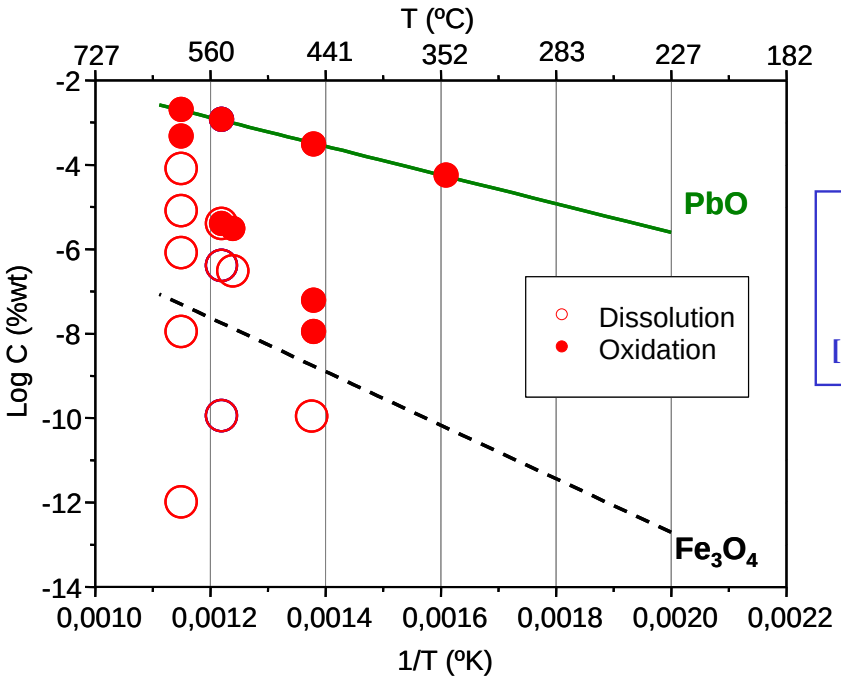

T^e = 350-600ºC

t = 100-3000 h

[O] = 10^{-12} wt.% – saturation

Figure 6.3.6. T91 steel in flowing LBE

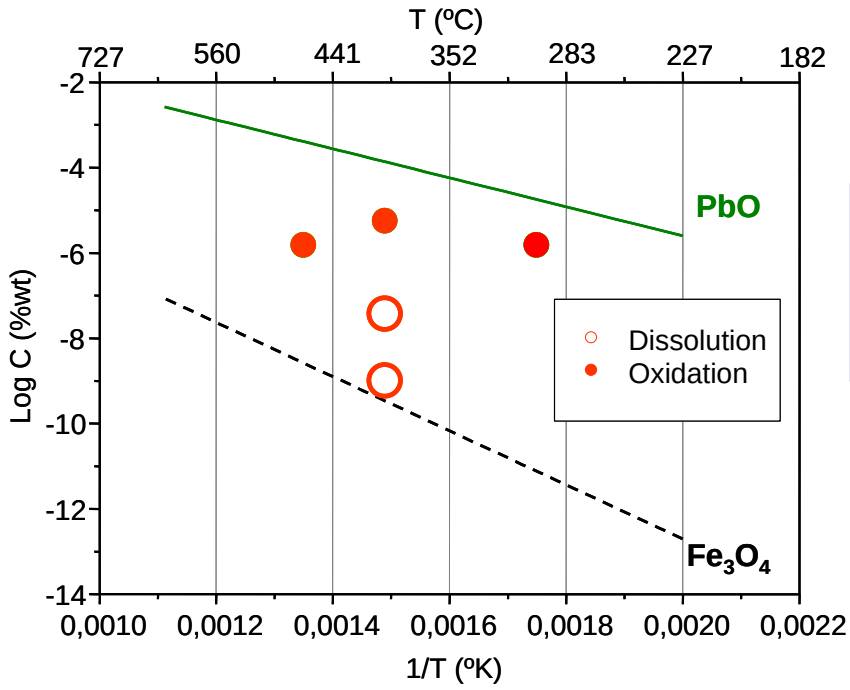

T^e = 300-470ºC

t = 1116-4500 h

[O] = 10^{-9}-10^{-5} wt.%

Figure 6.3.7. AISI 316L steel in stagnant LBE

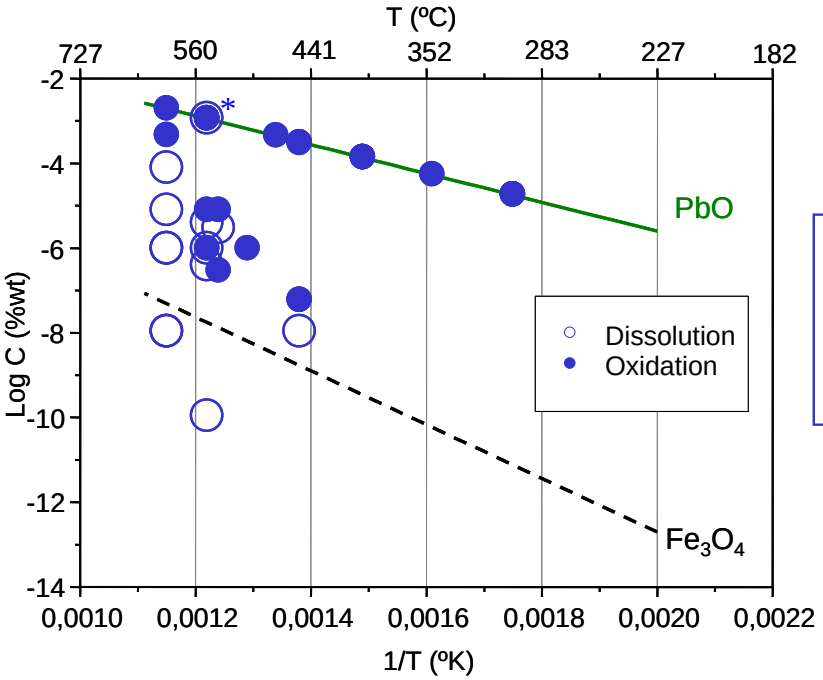

T^e = 300-600ºC

t = 100-10000 h

[O] = 10^{-10} wt.% – saturation

Figure 6.3.8. AISI 316L steel in flowing LBE

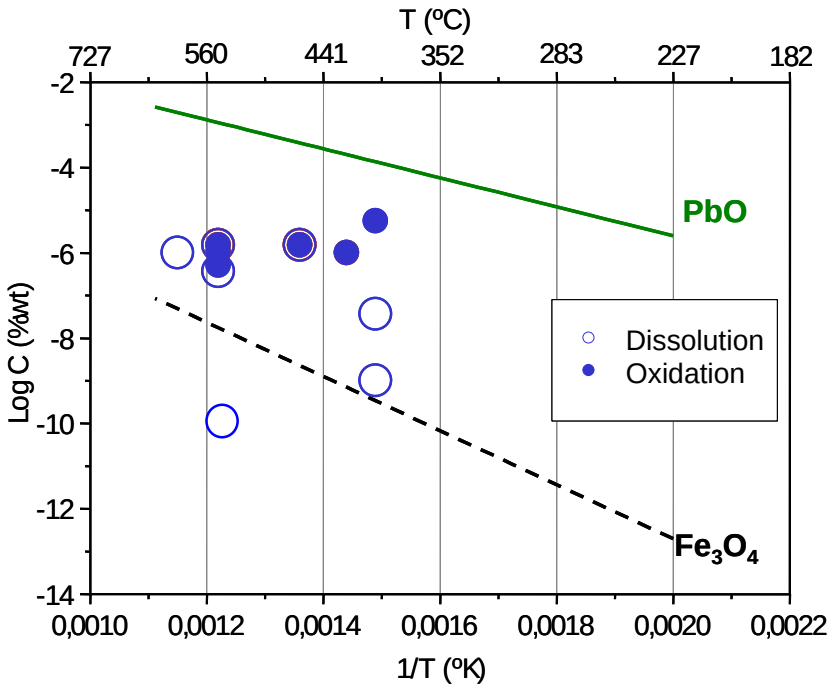

T^e = 400-600ºC

t = 959-7200h

[O] = 10^{-9}-10^{-5} wt.%

Figure 6.3.9. Steels in stagnant Pb

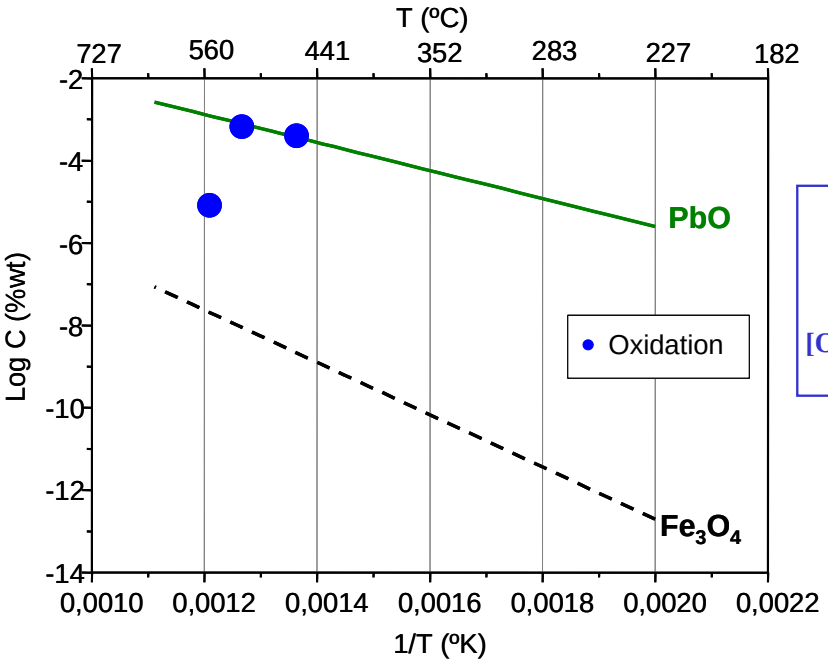

T^e = 464-550°C

t = 700-3700h

[O] = 8×10^{-6} wt.% – saturation

Figure 6.3.10. Steels in flowing Pb

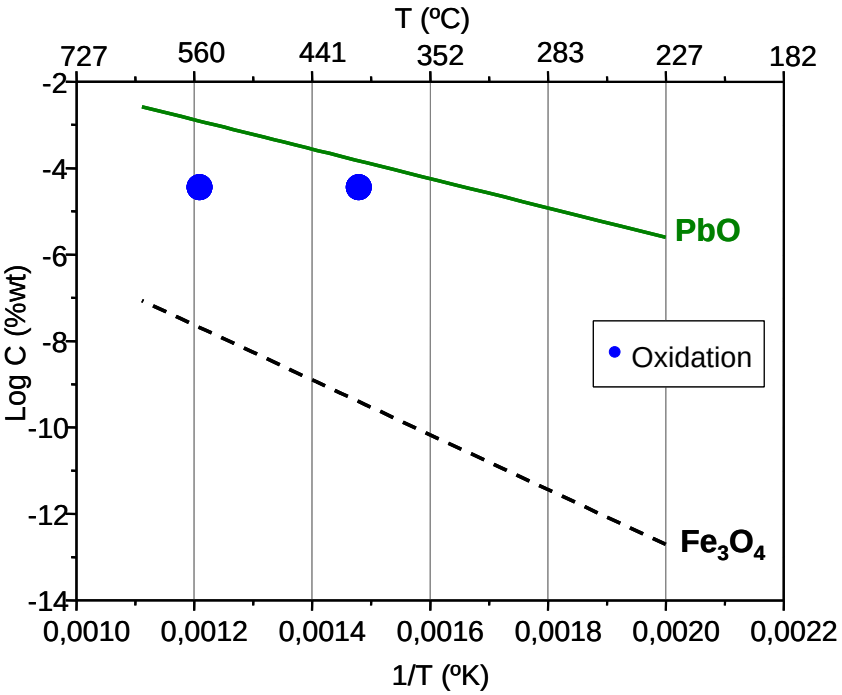

T^e = 400-550°C

t = 1027-3027h

[O] = 3-4 10^{-5} wt.%

6.4 Conclusions and further data needed

For tests conducted both in stagnant and in dynamic (flowing) LBE/Pb within the oxygen control band, most Fe-Cr and Fe-Cr-Ni steels form oxides that are protective below temperatures in the range 500-550°C, specially for an oxygen concentration above 10^{-6} wt.% for short- to medium-term applications.

Austenitic steels show thinner oxide layers. For oxygen concentrations lower than 10^{-6} wt.%, dissolution takes place in most of the steels, especially austenitic steels, due to the high solubility of nickel in LBE/Pb. For tests temperatures higher than 550°C, the formation and protectiveness of oxides is uncertain, and protection usually fails due to dissolution for long times.

Similar compositions of the oxide layers formed in Pb-Bi and Pb experiments have been described by several authors. In general, the steels show a double oxide layer formed by an outer layer with a composition comparable to that of magnetite and an inner layer where Cr content is higher than in the material bulk. The composition of this inner layer correspond to $Fe(Fe_{1-x}Cr_x)_2O_4$.

Further data needed

As was pointed out in this chapter, the existing data base for the corrosion of materials in LBE/Pb is very sparse in some areas. Additionally, the actual environment that existed during many of the reported test results is open to question. For example, it would seem to be improbable that dissolution would be the dominant corrosion mechanism for a stainless steel exposed at oxygen potentials near the PbO potential. Lastly, the state of the art of oxygen potential measurement is rapidly improving but for many of the reported test data, poorly measured. Thus, it is expected that much more data will be needed in the future in order to assure adequate system design. To this end, additional data is required in the following areas:

- Long-term tests (15000 hours) in dynamic conditions to confirm the actual oxygen-temperature areas, especially for T91 and 316L steels to support the design of future systems in which these steels have been chosen as reference.
- Tests in stagnant and flowing lead to expand the database in Pb at high temperature
- Influence of several parameters (surface state of steels, stresses, welding, etc.) on the corrosion response of steels to improve the knowledge about the dissolution/oxidation process and to support models and mechanisms.
- For high temperature systems (above 550°C), development and testing of advanced materials will be also needed.

6.5 Recommendations on corrosion tests procedure (standardisation)

Analysis of the available data indicates that a wide range of experimental conditions have been tested: temperatures from 300 to 650°C, times from 100 to 10000 hours and oxygen concentration in LBE/Pb from 10^{-12} wt.% to saturation.

Thirteen Fe-Cr steels and eleven Ni alloys have been tested. However, there are not enough data for each condition and, in some cases, not all the experimental conditions are reported. The result has been that much of the data cannot be properly interpreted. This indicates that it is necessary a more systematic work to be able to standardise the test procedures, but it is possible to give some general recommendations.

The approach to testing in LBE or Pb involves design and placement of samples, design of test system, the control and monitoring of tests conditions and the measurement and evaluation of corrosion damage. The general recommendations that follow are based on [Bagnall, 1995].

In order to assure valid results, tests should be well documented, and the following systematic parameters should be reported.

6.5.1 Pre-test preparation

6.5.1.1 Liquid metal: LBE and Pb

- Impurity analysis of the LBE or Pb should be made before and after each test.
- Total mass of LBE/Pb.

6.5.1.2 Material

- Composition.
- Thermo-mechanical treatment.
- Type of product.
- Mechanical and microstructure characteristics (hardness, etc.).
- Shape.
- Length.
- Thickness.
- Mass.
- Surface preparation: as mechanised, ground, electrolytic polished, etc. The test specimens should start its period of exposure with relatively smooth and readily reproducible surface conditions. The surface finishing should not introduce metallurgical changes in the surface.

The samples should be correctly identified using a technique that will not be destroyed during the test.

6.5.2 Test conditions

The compatibility of materials with heavy liquid metals can be studied using static, thermal convection and forced convection conditions. A detailed description of the typical systems is included in Chapter 12.

6.5.2.1 Static (no flow) tests

In isothermal devices for tests in stagnant LBE/Pb, the container can serve as test specimen, or the test specimen can be incorporated. In any case, the container and test specimen should be either of the same composition or, better, the container should be inert to corrosion in liquid metals. Relative surface areas of different metals and surface/liquid metal volume ratios are important points to consider

when designing small scale tests to examine corrosion trends. The liquid metal volume to exposed area metal ratio should be high enough to avoid saturation of main steel elements in the liquid metal. In general, materials with large compositional differences should not be exposed together to determine relative corrosion behaviour.

Temperature should be uniform in the liquid metal contained in the device. The oxygen content in LBE or Pb should be homogenised and known during the test period.

Stagnant tests are very useful to give a first screening of experimental conditions and contribute to the establishment of a corrosion mechanism in LBE/Pb. However, in isothermal conditions, the rate of dissolution reaction would decrease with time as the concentration of the main steel elements dissolved in the liquid metal increases. After a period of time, the actual elemental concentration becomes equal to the solubility and the dissolution rate is zero.

6.5.2.2 Dynamic tests

The simplest non-isothermal flowing system where processes associated with dissolution and deposition occur is one in which flow is induced by thermal convection. This is accomplished by heating one leg of a closed loop and cooling another leg. The flow rate is dependent on the height of the heated and cooled sections, on the temperature gradient and on the physical properties of the liquid. Thermal convection loops can be destructively examined after operation and specimens can be removed and replaced numerous times for cumulative periods without interruption of liquid metal flow. However, the utility of thermal convection loops is limited by the low flow velocities that can practically be achieved (maximum of about 60 mm/s), making extrapolations to the higher velocities in operating systems doubtful.

Higher flow velocities are obtained in forced convection loops where the liquid is pumped through the loop with an electromagnetic or mechanical pump. Test specimens of various materials are generally placed in the hot leg and the effect of the flowing liquid on the specimen is determined from changes in weight, dimensions, mechanical properties, and microstructure. Such an approach yields data on maximum corrosion rates as a function of temperature and liquid metal flow rate. The chemical balance between dissolution and deposition is strongly influenced by all materials (i.e. containment and tests specimens) exposed to the circulating LBE or Pb. The containment material has its own effect on test results in systems in which dissimilar metals or alloys are involved.

The parameters that should be taken into account during tests under flowing LBE or Pb are:

- *Materials*. Steel composition of the loop and test specimens must be analysed and reported. The test specimen distribution in the loop should always be given in detail when reporting corrosion results. Relative corrosion sources and sinks are of vital importance in the analysis of corrosion specimens.
- *Temperature*. Maximum and minimum temperature of the loop must be measured and reported during the loop operation. However, corrosion rate/temperature relationships are strongly influenced by system geometry. For this reason, loop geometry and temperature distribution along the loop should be also measured and reported during a test.
- *Flow rate*. In general, flow rate influences corrosion rate by LBE or Pb. If the liquid metal is flowing at high velocity, the structural materials could be also subject to erosion. It is necessary to measure and report the flow rate at several points of the loop, especially at the test sections.

- *Time*. Accurate kinetic measurements must be made over an extended time period for useful comparison and predictive analysis. The proposed exposure intervals are 2000, 5000, 10000 and 15000 hours. Accelerated corrosion takes place in the first hours of exposure, depending on the material and temperature, but 2000 hours seems a reasonable time to detect this period. After this initial period, a steady-state corrosion rate is usually attained. Accurate kinetic measurements must be made over an extended time period for useful comparisons and predictive analysis.
- *Oxygen concentration in LBE or Pb*. Corrosion inhibition is dependent on formation of protective surface films and control of oxygen in the liquid metal is essential for this process. The oxygen control system used to adjust and assure the required oxygen in the LBE or Pb – gas mixture, H_2/H_2O equilibrium or solid PbO – should be always reported. The knowledge of the oxygen concentration in the LBE or Pb is mandatory. This value, together with temperature, will give the valid area of operation.

6.5.3 Post-test analysis

The development of a common criteria to quantify LBE or Pb effects on materials is essential for comparison of results from different labs and to reach conclusions. In general, the corrosion damage and the oxidation observed is heterogeneous, with simultaneous existence of dissolution areas and oxidation protected areas. In these cases, weight change measurements alone could lead to erroneous interpretation. There is not a single method reliable for all the cases. For comparison, one should perform metallographic examination, weight change measurements and try to measure the remaining unaffected thickness of interior bulk.

- Metallographic examination. Cross-section of the tested steels without removal of the remaining LBE or Pb should be used for the analysis of the oxide layer formed on the surface or the morphology of dissolution and its depth. The oxide layer should be characterised focussing on the following parameters:
  - *Thickness*. It should be measured at several zones and give a medium value.
  - *Structure*. Indicate porosity, adherence, hardness, etc.
  - *Composition*. Indicate enrichment or depletion of the main steel elements.
  - *General aspect*. LBE/Pb penetration, spalling, etc. It is useful to attach a photograph.

  All these items should be reported.
- Weight change measurements. For this method, the removal of solidified LBE or Pb from the test specimen without damaging the surface or destroying a layer or deposit is required. The methodology of cleaning – mercury or silicone baths at a certain temperature, etc. – must be reported. The use of mercury is not recommended since it is highly hazardous.

Table 6.3.1. Composition of Fe-Cr steels

	SCM 420	2,25Cr-1Mo	F82H	STBA 28	T91	NF 616	ODS-M	Eurofer 97	STBA 26	Optifer IVc	EM10	Manet II	56T5	12CR	ODS	EP823	HT9	HCM 12A	HCM 12	410ss	T410	430ss
C		0.100-11	0.10-0.095	0.10	0.1-0.11		0.13	0.12		0.13	0.1-0.097	0.11	0.20	0.11		0.14-0.18	0.22			0.067		0.08
Cr	1.2	2.18-2.25	7.70-7.75	8.41-8.6	8.26-8.63	8.8-9	8.85	8.93	9	9.05	8.8-9.15	10.3	10.51	10.54	11.72	10.97-12	12	12	12.1	12.21	12.5	16.24
Ni		0.02	0.015	0.06	0.13-0.23		0.01	0.022			0.04-0.2	0.68	0.66	0.33		0.75-0.89	0.59			0.12	0.34	0.15
Mo	0.2	0.92-1.00	0.010	0.88-1	0.91-0.95	0.3-0.5		0.0015	1		0.97-1	0.61	0.65	0.34		0.7-0.73	1.11	0.3	1.1	0.02		0.02
W			1.94-2.10		<0.01	1.8-1.9	1.94	1.07		1	0.005			1.76	1.99	0.64-1.2	0.5	1.9	1			
Mn		0.44-0.55	0.01-0.16	0.40	0.43-0.78	0.5	<0.01	0.47	0.3-0.43	0.52	0.5	0.78	0.61	0.64		0.59-0.67	0.58	0.5	0.5	0.80	1	0.23
Si	0.2	0.34	0.1-0.23	0.30-0.40	0.31-0.43	0.3	<0.005	0.06	0.20-0.43		0.37-0.44		0.22	0.27		1.21-1.8	0.30	0.3	0.3	0.31	1	0.52
P		<0.035			0.01-0.02		0.001	0.005			0.0042	0.003		0.016								
S		<0.030	0.003		0.0030.006		0.003	0.004			<0.001			0.002								
Cu			0.01-0.03		0.19-0.05			0.0036			0.055			1								
Al		0.002	0.004		<0.01			0.008			<0.005			0.001						0.002		0.007
Nb			<0.01	0.08	0.07-0.09	0.07		0.0022			0.01	0.14	0.48	0.048		0.34-0.4		0.05	0.09			
Co			3×10^{-3}		0.02			0.0036			0.03											
V		0.01	0.14-0.18	0.20	0.20-0.23	0.2		0.20		0.25	0.032	0.20	0.18	0.19		0.33-0.43		0.2	0.3	0.07		0.10
Ti		<0.01	0.004-0.01	0.033	0.003		0.2				0.01				0.29					<0.01		<0.01
N		0.009	0.010	0.047	0.04		0.011	0.018			0.014			0.071						0.013		0.024
B			4×10^{-4}		<0.0005						<0.001			0.034								
Y							0.27								0.4							

Table 6.3.2. Composition of austenitic steels

	D9	14Cr-16Ni-2Mo	1.4970	316L	1.4984	304L
C	0.04	0.058	0.46	0.012-0.02	0.06	0.020
Cr	13.6	14.14	16.5	16-18	17-19	18.50
Ni	13.6	15.85	13.8	10-17.392	10-12	8.31
Mo	1.67	2.29	0.66	2-2.75		0.39
Mn	2.1	1.54	1.91	0.2-2	0-2	1.67
Si	0.85	0.50	0.89	0.1-1	0-0.75	0.49
P			0.012	0.024-0.19		0.026
S			0.009	0.0005-0.03		0.003
Co				0.06-0.14		
N		0.003		0.02-0.1		0.069
Ti	0.30	0.22	0.43			
V		0.03				
W		0.010				
Al		0.012				

Table 6.3.3. Fe-Cr steels in stagnant LBE

Material	T (°C)	Time (hours)	[O] (%wt.)	OCS	Surface sample/LBE volume ratio (cm^2/l)	Oxide thickness/ dissolution depth (microns)	Remark 1	Remark 2	Ref.
F82H	476	700	Saturation	Argon		18	Oxidation		[Fazio, 2001]
F82H	476	1200	Saturation	Argon		34	Oxidation		[Fazio, 2001]
F82H*	400	100		Argon	9.7/0.035		Oxidation	Weight gain: -3 mdd[1]	[Soler, 2001]
F82H*	600	100		Argon	9.7/0.035			Weight loss:36 mdd	[Soler, 2001]
F82H*	600	665		Argon	9.7/0.035			Weight loss: 52 mdd	[Soler, 2001]
F82H-preox.*	400	100		Argon	9.7/0.035			Weight loss: 4 mdd	[Soler, 2001]
F82H-preox.*	600	100		Argon	9.7/0.035			Weight loss: 14 mdd	[Soler, 2001]
F82H-preox.*	600	665		Argon	9.7/0.035			Weight loss: 2.5 mdd	[Soler, 2001]
F82H*	400	100		Argon + 10%H_2	9.7/0.035			Weight gain: -1 mdd	[Soler, 2001]
F82H*	600	100		Argon + 10%H_2	9.7/0.035			Weight loss: 3 mdd	[Soler, 2001]
F82H*	600	665		Argon + 10%H_2	9.7/0.035			Weight loss: 11 mdd	[Soler, 2001]
F82H-preox.*	400	100		Argon + 10%H_2	9.7/0.035			Weight loss: 2 mdd	[Soler, 2001]
F82H-preox.*	600	100		Argon + 10%H_2	9.7/0.035			Weight loss: 17 mdd	[Soler, 2001]
F82H-preox.*	600	665		Argon + 10%H_2	9.7/0.035			Weight loss: 2 mdd	[Soler, 2001]
F82H	550	500	Saturation	Ar	10.8/	20	Oxidation		[Kurata, 2002]
F82H	535	1000	3×10^{-7}	Ar-H_2/H_2O	5/0.004	20	Oxidation		[Gómez, 2002]
F82H	550	500, 1000	4×10^{-7}	Ar-H_2/H_2O	5/0.004		Dissolution	Coexistence with oxide	[Gómez, 2002]
F82H	535	500	3×10^{-7}	Ar-H_2/H_2O	5/0.004	15	Oxidation		[Gómez, 2002]
F82H	550	100	4×10^{-7}	H_2/H_2O	5/0.004	-18	Dissolution		[Martín, 2004]
F82H	600	100	8×10^{-7}	H_2/H_2O	5/0.004	-5	Dissolution		[Martín, 2004]
F82H	535	3000	3×10^{-7}	H_2/H_2O	5/0.004	-13	Dissolution	Rests of oxide layer	[Martín, 2004]
F82H	550	3000	4×10^{-7}	H_2/H_2O	5/0.004	-17	Dissolution	No rests of oxide layer	[Martín, 2004]
F82H	535	500	3×10^{-6}	H_2/H_2O	5/0.004	8	Oxidation		[Martín, 2004]
F82H	550	500	4×10^{-6}	H_2/H_2O	5/0.004	14	Oxidation		[Martín, 2004]
F82H	600	500	8×10^{-6}	H_2/H_2O	5/0.004	-21	Dissolution	Rests of oxide layer (Cr enrichment)	[Martín, 2004]
F82H	535	3000	3×10^{-6}	H_2/H_2O	5/0.004	-10	Dissolution		[Martín, 2004]
F82H	550	3000	4×10^{-6}	H_2/H_2O	5/0.004	-5	Dissolution		[Martín, 2004]
F82H	600	3000	8×10^{-5}	H_2/H_2O	5/0.004	-80	Dissolution	Coexistence with oxide layer	[Martín, 2004]
F82H	450	3000	6×10^{-8}	H_2/H_2O	5/0.004	11	Oxidation	Oxide layer detached in zones	[Gómez, 2004]
F82H-preox	450	3000	6×10^{-8}	H_2/H_2O	5/0.004	14	Oxidation	Oxide layer broken in some zones	[Gómez, 2004]

Table 6.3.3. Fe-Cr steels in stagnant LBE (*cont.*)

Material	T (°C)	Time (hours)	[O] (%wt.)	OCS	Surface sample/LBE volume ratio (cm^2/l)	Oxide thickness/ dissolution depth (microns)	Remark 1	Remark 2	Ref.
F82H	600	100	4.7×10^{-4}	$Ar + H_2 + H_2O$	9.7/0.035	17	Oxidation		[Soler, 2004]
F82H	600	500	4.7×10	$Ar + H_2 + H_2O$	9.7/0.035	48	Oxidation		[Soler, 2004]
F82H	600	1500	4.7×10	$Ar + H_2 + H_2O$	9.7/0.035	90	Oxidation		[Soler, 2004]
F82H	600	100	2×10^{-3}	Ar (saturation)	9.7/0.035	13	Oxidation		[Soler, 2004]
F82H	600	500	2×10^{-3}	Ar (saturation)	9.7/0.035	35	Oxidation		[Soler, 2004]
F82H	600	1500	2×10^{-3}	Ar (saturation)	9.7/0.035	24	Oxidation	Pb-Bi penetration	[Soler, 2004]
F82H	450	100	6×10^{-8}	H_2/H_2O	9.7/0.035		Oxidation	Cr oxide, discontinuous oxide	[Soler, 2004]
F82H	450	500	3×10^{-4}	Ar (saturation)	9.7/0.035	4	Oxidation		[Soler, 2004]
F82H	450	1500	6×10^{-8}	H_2/H_2O	9.7/0.035		Oxidation	Cr oxide	[Soler, 2004]
F82H	600	500	1.1×10^{-8}	$Ar + H_2$	9.7/0.035		Oxidation	Coexistence of dissolution and oxidation	[Soler, 2004]
F82H	600	100	1.1×10^{-8}	H_2/H_2O	9.7/0.035	15	Oxidation		[Soler, 2004]
F82H	600	1500	1.1×10^{-8}	H_2/H_2O	9.7/0.035	-40	Dissolution		[Soler, 2004]
F82H	450	500, 2400	1.1×10^{-8}	$Ar + H_2$	9.7/0.035		Oxidation	Cr oxidation	[Soler, 2004]
F82H	600	1500	1.1×10^{-8}	$Ar + H_2$	9.7/0.035		Dissolution		[Soler, 2004]
F82H	450	3000	3.2×10^{-4}	Ar-saturation	21.6/0.7	8.39			[Kurata, 2005]
F82H	550	3000	1.2×10^{-3}	Ar-saturation	21.6/0.7	13.95	Oxidation	Internal oxidation (6.19 μm)	[Kurata, 2005]
Mod9Cr-1Mo	450	3000	3.2×10^{-4}	Ar-saturation	21.6/0.7	8.41	Oxidation		[Kurata, 2005]
Mod9Cr-1Mo	550	3000	1.2×10^{-3}	Ar-saturation	21.6/0.7	13.97	Oxidation	Internal oxidation (7.32 μm)	[Kurata, 2005]
9Cr-1Mo	550	500	Saturation	Ar	10.8/	20	Oxidation		[Kurata, 2002]
T91	550	100	4×10^{-7}	H_2/H_2O	5/0.004	-16	Dissolution		[Martín, 2004]
T91	600	100	8×10^{-7}	H_2/H_2O	5/0.004	-5	Dissolution		[Martín, 2004]
T91	535	3000	3×10^{-7}	H_2/H_2O	5/0.004	-26	Dissolution		[Martín, 2004]
T91	550	3000	4×10^{-7}	H_2/H_2O	5/0.004	-34			[Martín, 2004]
T91	535	500	3×10^{-6}	H_2/H_2O	5/0.004	18	Oxidation	Broken and detached	[Martín, 2004]
T91	550	500	4×10^{-6}	H_2/H_2O	5/0.004	17	Oxidation		[Martín, 2004]
T91	600	500	8×10^{-6}	H_2/H_2O	5/0.004	-21	Dissolution	Rest of oxide layer (Cr enrichment)	[Martín, 2004]
T91	535	3000	3×10^{-6}	H_2/H_2O	5/0.004			No oxidation/no dissolution	[Martín, 2004]

Table 6.3.3. Fe-Cr steels in stagnant LBE (*cont.*)

Material	T (°C)	Time (hours)	[O] (%wt.)	OCS	Surface sample/LBE volume ratio (cm^2/l)	Oxide thickness/ dissolution depth (microns)	Remark 1	Remark 2	Ref.
T91	550	3000	4×10^{-6}	H_2/H_2O	5/0.004	-20	Dissolution		[Martín, 2004]
T91	600	3000	8×10^{-5}	H_2/H_2O	5/0.004	-130	Dissolution	Coexistence with oxide layer	[Martín, 2004]
T91	450	3000	6×10^{-8}	H_2/H_2O	5/0.004	30	Oxidation	Broken oxide layer	[Gómez, 2004]
T91 preox	450	3000	6×10^{-8}	H_2/H_2O	5/0.004	12	Oxidation	Broken in some zones	[Gómez, 2004]
T91	600	100	4.7×10^{-4}	$Ar + H_2 + H_2O$	9.7/0.035	20	Oxidation		[Soler, 2004]
T91	600	500	4.7×10^{-4}	$Ar + H_2 + H_2O$	9.7/0.035	41	Oxidation		[Soler, 2004]
T91	600	1500	4.7×10^{-4}	$Ar + H_2 + H_2O$	9.7/0.035	95	Oxidation		[Soler, 2004]
T91	600	100	2×10^{-3}	Ar (saturation)	9.7/0.035	10	Oxidation		[Soler, 2004]
T91	600	500	2×10^{-3}	Ar (saturation)	9.7/0.035	32	Oxidation		[Soler, 2004]
T91	600	1500	2×10^{-3}	Ar (saturation)	9.7/0.035	40	Oxidation	Pb-Bi penetration	[Soler, 2004]
T91	450	500	3×10^{-4}	Ar (saturation)	9.7/0.035	6	Oxidation		[Soler, 2004]
T91	450	100	6×10^{-8}	H_2/H_2O	9.7/0.035		Oxidation	Cr oxide, discontinuous oxide	[Soler, 2004]
T91	450	1500	6×10^{-8}	H_2/H_2O	9.7/0.035	5	Oxidation		[Soler, 2004]
T91	600	100	1.1×10^{-8}	H_2/H_2O	9.7/0.035	22	Oxidation		[Soler, 2004]
T91	600	1500	1.1×10^{-8}	H_2/H_2O	9.7/0.035	-10	Dissolution		[Soler, 2004]
T91	450	500, 2400	1.1×10^{-8}	$Ar + H_2$	9.7/0.035		Oxidation	Cr oxidation	[Soler, 2004]
T91	600	500	1.1×10^{-8}	$Ar + H_2$	9.7/0.035	5	Oxidation	Thin oxidation	[Soler, 2004]
T91	600	1500	1.1×10^{-8}	$Ar + H_2$	9.7/0.035	-13	Dissolution		[Soler, 2004]
T91	450	550	3.14×10^{-4}	Ar N60	4/	10	Oxidation		[Gnecco, 2004]
T91	550	550	1.17×10^{-3}	Ar N60	4/	7	Oxidation		[Gnecco, 2004]
T91*	600	550		Ar N60	4/	14	Oxidation		[Gnecco, 2004]
T91*	350	1000		Ar N60	4/	2	Oxidation		[Gnecco, 2004]
T91*	450	1000		Ar N60	4/	12	Oxidation		[Gnecco, 2004]
T91	550	1000	1.17×10^{-3}		4/	10	Oxidation		[Gnecco, 2004]
T91*	600	1000		Ar N60	4/	3-4	Oxidation		[Gnecco, 2004]
T91	550	550	3.9×10^{-9}	$Ar + 5\%H_2$	4/	-7	Dissolution		[Gnecco, 2004]
T91	450	2000	3.9×10^{-9}	$Ar + 5\%H_2$	4/	-3	Dissolution		[Gnecco, 2004]
T91	550	2000	3.9×10^{-9}	$Ar + 5\%H_2$	4/	-30	Dissolution		[Gnecco, 2004]
T91	470	7800	Saturation			30	Oxidation		[Martinelli, 2005]
12Cr,ODS-M	500	800	1×10^{-6}	$Ar\text{-}H_2/H_2O$			Oxidation		[Furukawa, 2004]

Table 6.3.3. Fe-Cr steels in stagnant LBE (*cont.*)

Material	T (°C)	Time (hours)	[O] (%wt.)	OCS	Surface sample/LBE volume ratio (cm^2/l)	Oxide thickness/ dissolution depth (microns)	Remark 1	Remark 2	Ref.
12Cr,ODS-M	500	2000	1×10^{-6}	Ar-H_2/H_2O			Oxidation	Diffusion+Fe-Cr-O+Fe-O+ porous Fe-O	[Furukawa, 2004]
12Cr,ODS-M	500	5000	1×10^{-6}	Ar-H_2/H_2O			Dissolution	Dissolution at some points	[Furukawa, 2004]
12Cr	550	800	1×10^{-6}	Ar-H_2/H_2O		15	Oxidation		[Furukawa, 2004]
12Cr	550	2000	1×10^{-6}	Ar-H_2/H_2O		25	Oxidation	Diffusion+Fe-Cr-O+Fe-O+ porous Fe-O	[Furukawa, 2004]
12Cr	550	5000	1×10^{-6}	Ar-H_2/H_2O		20	Dissolution	Dissolution at some points	[Furukawa, 2004]
12Cr,ODS-M	600	800, 5000	1×10^{-6}	Ar-H_2/H_2O					[Furukawa, 2004]
12Cr,ODS-M	600	2000	1×10^{-6}	Ar-H_2/H_2O			Dissolution	Coexist with Fe-Cr-O	[Furukawa, 2004]
12Cr,ODS-M	650	800	1×10^{-6}	Ar-H_2/H_2O			Oxidation	Fe-O + Fe-Cr-O	[Furukawa, 2004]
12Cr,ODS-M	650	2000	1×10^{-6}	Ar-H_2/H_2O			Dissolution		[Furukawa, 2004]
12Cr,ODS-M	650	5000	1×10^{-6}	Ar-H_2/H_2O					[Furukawa, 2004]
ODS-M	550	800	1×10^{-6}	Ar-H_2/H_2O		20			[Furukawa, 2004]
ODS-M	550	2000	1×10^{-6}	Ar-H_2/H_2O		30	Oxidation	Diffusion + Fe-Cr-O + Fe-O + porous Fe-O	[Furukawa, 2004]
ODS-M	550	5000	1×10^{-6}	Ar-H_2/H_2O		30	Dissolution	Dissolution at some points	[Furukawa, 2004]
Eurofer 97	550	550	1.17×10^{-3}	Ar N60	4/	6	Oxidation		[Gnecco, 2004]
EM10	550	100	4×10^{-7}	H_2/H_2O	5/0.004	-14	Dissolution		[Martín, 2004]
EM10	535	3000	3×10^{-7}	H_2/H_2O	5/0.004	-45	Dissolution		[Martín, 2004]
EM10	550	3000	4×10^{-7}	H_2/H_2O	5/0.004	-65	Dissolution		[Martín, 2004]
EM10	535	500	3×10^{-6}	H_2/H_2O	5/0.004	14	Oxidation		[Martín, 2004]
EM10	550	500	4×10^{-6}	H_2/H_2O	5/0.004	10	Oxidation		[Martín, 2004]
EM10	600	500	8×10^{-6}	H_2/H_2O	5/0.004	-21	Dissolution	Rest of oxide layer (Cr enrichment)	[Martín, 2004]
EM10	535	3000	3×10^{-6}	H_2/H_2O	5/0.004	-10	Dissolution		[Martín, 2004]
EM10	550	3000	4×10^{-6}	H_2/H_2O	5/0.004	-15	Dissolution		[Martín, 2004]
EM10	600	3000	8×10^{-5}	H_2/H_2O	5/0.004	-16	Dissolution	Coexistence with oxide layer	[Martín, 2004]
EM10	450	3000	6×10^{-8}	H_2/H_2O	5/0.004	11	Oxidation	Oxide layer detached in zones	[Gómez, 2004]
EM10-preox	450	3000	6×10^{-8}	H_2/H_2O	5/0.004	9	Oxidation	Broken in some zones	[Gómez, 2004]
EM10	600	100	4.7×10	Ar + H_2 + H_2O	9.7/0.035	22	Oxidation		[Soler, 2004]
EM10	600	500	4.7×10	Ar + H_2 + H_2O	9.7/0.035	41	Oxidation		[Soler, 2004]
EM10	600	1500	4.7×10	Ar + H_2 + H_2O	9.7/0.035	95	Oxidation		[Soler, 2004]

Table 6.3.3. Fe-Cr steels in stagnant LBE (*cont.*)

Material	T (°C)	Time (hours)	[O] (%wt.)	OCS	Surface sample/LBE volume ratio (cm^2/l)	Oxide thickness/ dissolution depth (microns)	Remark 1	Remark 2	Ref.
EM10	600	100	2×10^{-3}	Ar (saturation)	9.7/0.035	9	Oxidation		[Soler, 2004]
EM10	600	500	2×10^{-3}	Ar (saturation)	9.7/0.035	37	Oxidation		[Soler, 2004]
EM10	600	1500	2×10^{-3}	Ar (saturation)	9.7/0.035	43	Oxidation	Pb-Bi penetration	[Soler, 2004]
EM10	450	500	3×10^{-4}	Ar (saturation)	9.7/0.035	4	Oxidation		[Soler, 2004]
EM10	450	100	6×10^{-8}	H_2/H_2O	9.7/0.035		Oxidation	Cr oxide	[Soler, 2004]
EM10	450	1500	6×10^{-8}	H_2/H_2O	9.7/0.035	7	Oxidation	Detached with dissolution underneath	[Soler, 2004]
EM10	600	100	1.1×10^{-8}	H_2/H_2O	9.7/0.035	15	Oxidation		[Soler, 2004]
EM10	600	1500	1.1×10^{-8}	H_2/H_2O	9.7/0.035	-10	Dissolution		[Soler, 2004]
EM10	450	500, 2400	1.1×10^{-8}	$Ar+H_2$	9.7/0.035		Oxidation	Cr oxidation	[Soler, 2004]
EM10	600	500	1.1×10^{-8}	$Ar+H_2$	9.7/0.035	2	Oxidation	Thin oxidation	[Soler, 2004]
EM10	600	1500	1.1×10^{-8}	$Ar+H_2$	9.7/0.035		Dissolution	Slight	[Soler, 2004]
Manet II	300	1500	Saturation	Argon		n.m.	Oxidation		[Fazio, 2001]
Manet II	300	5000	Saturation	Argon		<1	Oxidation		[Fazio, 2001]
Manet II	400	1500	Saturation	Argon		1	Oxidation		[Fazio, 2001]
Manet II	400	5000	Saturation	Argon		5	Oxidation		[Fazio, 2001]
Manet II	476	700	Saturation	Argon		11	Oxidation		[Fazio, 2001]
Manet II	476	1200	Saturation	Argon		16	Oxidation		[Fazio, 2001]
Manet II	300	1500, 3000, 5000	1.84×10^{-5}	Argon			Oxidation	Thin	[Benamati, 2002]
Manet II	400	1500, 3000	1.41×10^{-4}	Argon			Oxidation	Thin	[Benamati, 2002]
Manet II	400	5000	1.41×10^{-4}	Argon			Oxidation	Thicker	[Benamati, 2002]
Manet II	550	1500	1.17×10^{-3}	Argon			Dissolution		[Benamati, 2002]
Manet II	550	3000, 5000	1.17×10^{-3}	Argon			Dissolution	Severe. Coexistence with thin oxide.	[Benamati, 2002]
Manet	300	1500, 3000	1.85×10^{-5}	Saturation			Oxidation	Thin	[Bin, 2003]
Manet	400	1500, 3000	1.41×10^{-4}	Saturation			Oxidation	Thin	[Bin, 2003]
Manet	550	1500	1.17×10^{-3}	Saturation			Dissolution	Coexistence with oxide layer	[Bin, 2003]

Table 6.3.3. Fe-Cr steels in stagnant LBE (*cont.*)

Material	T (°C)	Time (hours)	[O] (%wt.)	OCS	Surface sample/LBE volume ratio (cm^2/l)	Oxide thickness/ dissolution depth (microns)	Remark 1	Remark 2	Ref.
Manet	550	3000, 5000	1.17×10^{-3}	Saturation			Dissolution		[Bin, 2003]
Manet	300	5000	1.85×10^{-5}	Saturation			Oxidation		[Bin, 2003]
Manet	400	5000	1.41×10^{-4}	Saturation			Oxidation	Double layer	[Bin, 2003]
56T5	>480	3000	5×10^{-7}		3.42/		Dissolution	Intergranular attack	[Deloffre, 2002]
56T5	400-480	3000	5×10^{-7}		3.42/			Fe deposits	[Deloffre, 2002]
56T5	<400	3000	5×10^{-7}		3.42/			No deposits	[Deloffre, 2002]
ODS	500	10000	10^{-6}	H_2/H_2O			Oxidation		[Furukawa, 2004]
ODS	550	5000	10^{-6}	H_2/H_2O			Oxidation		[Furukawa, 2004]
ODS	600	2000	10^{-6}	H_2/H_2O			Oxidation	Spinel + dissolution zones	[Furukawa, 2004]
ODS	650	2000	10^{-6}	H_2/H_2O			Oxidation	Spinel + dissolution zones	[Furukawa, 2004]
ODS	650	5000	10^{-6}	H_2/H_2O			Dissolution	partial	[Furukawa, 2004]
ODS	650	10000	10^{-6}	H_2/H_2O			Dissolution		[Furukawa, 2004]
ODS	650	5000	10^{-4}	H_2/H_2O			Oxidation	Rehealing	[Furukawa, 2004]
ODS	650	2000	10^{-8}	H_2/H_2O			Oxidation		[Furukawa, 2004]
ODS	650	5000	10^{-8}	H_2/H_2O			Oxidation	LBE inclusion pores	[Furukawa, 2004]
HT9	500	800	1×10^{-6}	H_2/H_2O		8	Oxidation	COSTA	[Müller, 2004]
HT9	500	2000	1×10^{-6}	H_2/H_2O			Oxidation	COSTA	[Müller, 2004]
HT9	500	5000	1×10^{-6}	H_2/H_2O		60-70	Oxidation	Porosity layer at the interface	[Müller, 2004]
HT9	550	800, 2000	1×10^{-6}	H_2/H_2O			Oxidation		[Müller, 2004]
HT9	550	5000	1×10^{-6}	H_2/H_2O		50	Oxidation		[Müller, 2004]
HT9	600	800, 2000	1×10^{-6}	H_2/H_2O			Oxidation		[Müller, 2004]
HT9	600	5000	1×10^{-6}	H_2/H_2O		50	Oxidation	Pb-Bi pentration	[Müller, 2004]
410ss	450	3000	3.2×10^{-4}	Ar-saturation	21.6/0.7	2.83	Oxidation		[Kurata, 2005]
410ss	550	3000	1.2×10^{-3}	Ar-saturation	21.6/0.7	5.42	Oxidation		[Kurata, 2005]
410ss, 430ss	550	500	Saturation	Ar	10.8/		Oxidation	Thin oxide layer	[Kurata, 2002]

* Not clarified enough (oxygen content information missed).

1. Milligrams/decimetre-day. 1 decimeter = 100 cm^2.

1. **Table 6.3.4. Fe-Cr-Ni steels in stagnant LBE**

Material	T (ºC)	Time (hours)	[O] (%wt.)	OCS	Surface sample/LBE volume ratio (cm^2/l)	Oxide thickness/ dissolution depth (microns)	Remark 1	Remark 2	Ref.
14Cr-16Ni-2Mo	550	500	Saturation	Argon	10.8/		Oxidation	Thin	[Kurata, 2002]
316L	300, 400	1500	Saturation	Argon		n.m.	Oxidation		[Fazio, 2001]
316L	300	5000	Saturation	Argon		<1	Oxidation		[Fazio, 2001]
316L	400	5000	Saturation	Argon		1	Oxidation		[Fazio, 2001]
316L	476	700	Saturation	Argon		n.m.	Oxidation		[Fazio, 2001]
316L	476	1200	Saturation	Argon		2-4	Oxidation		[Fazio, 2001]
316L	300	1500, 3000, 5000	1.84×10^{-5}	Argon			Oxidation	Thin	[Benamati, 2002]
316L	400	1500, 3000, 5000	1.41×10^{-4}	Argon			Oxidation	Thin	[Benamati, 2002]
316L	550	1500	1.17×10^{-3}	Argon			Oxidation	Thin-spongy	[Benamati, 2002]
316L	550	3000,5000	1.17×10^{-3}	Argon			Dissolution	Pb-Bi penetration	[Benamati, 2002]
316L–Preox.	>450	3000	5×10^{-7}		3.42/	10-35	Oxidation	Porous layer	[Deloffre, 2002]
316L	360-450	3000	5×10^{-7}		3.42/		Oxidation	Crystals. Fe rich at high T, Cr rich at low T.	[Deloffre, 2002]
316L	<360	3000	5×10^{-7}		3.42/		Oxidation	No deposits	[Deloffre, 2002]
316FBR	500	800, 200, 5000	1×10^{-6}	Ar-H_2/H_2O					[Furukawa, 2004]
316FBR	550	800	1×10^{-6}	Ar-H_2/H_2O		10	Oxidation	Fe-O	[Furukawa, 2004]
316FBR	550	2000	1×10^{-6}	Ar-H_2/H_2O		20	Oxidation	Fe-O	[Furukawa, 2004]
316FBR	550	5000	1×10^{-6}	Ar-H_2/H_2O					[Furukawa, 2004]
316FBR	600	800, 2000	1×10^{-6}	Ar-H_2/H_2O			Dissolution	+ Cr_2O_3	[Furukawa, 2004]
316FBR	600	5000	1×10^{-6}	Ar-H_2/H_2O					[Furukawa, 2004]
316FBR	650	800, 2000, 5000	1×10^{-6}	Ar-H_2/H_2O					[Furukawa, 2004]
316L	550	100	4×10^{-7}	H_2/H_2O	5/0.004	-9	Dissolution		[Martín, 2004]
316L	535	3000	3×10^{-7}	H_2/H_2O	5/0.004		Oxidation	Oxide nodules	[Martín, 2004]
316L	550	3000	4×10^{-7}	H_2/H_2O	5/0.004	-46	Dissolution		[Martín, 2004]
316L	535	500	8×10^{-6}	H_2/H_2O	5/0.004	11	Oxidation		[Martín, 2004]

Table 6.3.4. Fe-Cr-Ni steels in stagnant LBE (*cont.*)

Material	T (ºC)	Time (hours)	[O] (%wt.)	OCS	Surface sample/LBE volume ratio (cm^2/l)	Oxide thickness/ dissolution depth (microns)	Remark 1	Remark 2	Ref.
316L	550	500	8×10^{-6}	H_2/H_2O	5 /0.004	9	Oxidation		[Martín, 2004]
316L	600	500	8×10^{-6}	H_2/H_2O	5 /0.004	-55	Dissolution		[Martín, 2004]
316L	535	3000	3×10^{-6}	H_2/H_2O	5 /0.004	-60	Dissolution		[Martín, 2004]
316L	550	3000	4×10^{-6}	H_2/H_2O	5 /0.004	-70	Dissolution		[Martín, 2004]
316L	600	3000	8×10^{-5}	H_2/H_2O	5 /0.004	-156	Dissolution		[Martín, 2004]
316L	450	3000	6×10^{-8}	H_2/H_2O	5 /0.004		Oxidation	Cr oxide	[Gómez, 2004]
316L-preox	450	3000	6×10^{-8}	H_2/H_2O	5 /0.004	4	Oxidation	Oxide nodules	[Gómez, 2004]
316L	600	100	4.7×10^{-4}	$Ar + H_2 + H_2O$	9.7/0.035	8	Oxidation		[Soler, 2004]
316L	600	500	4.7×10^{-4}	$Ar + H_2 + H_2O$	9.7/0.035	27	Oxidation		[Soler, 2004]
316L	600	1500	4.7×10^{-4}	$Ar + H_2 + H_2O$	9.7/0.035	45	Oxidation		[Soler, 2004]
316L	600	100	2×10^{-3}	Ar-saturation	9.7/0.035	0.3	Oxidation	Oxide nodules 7	[Soler, 2004]
316L	600	500	2×10^{-3}	Ar-saturation	9.7/0.035	24	Oxidation		[Soler, 2004]
316L	600	1500	2×10^{-3}	Ar-saturation	9.7/0.035	15	Oxidation		[Soler, 2004]
316L	450	500	3×10^{-4}	Ar-saturation	9.7/0.035		Oxidation	Cr oxide	[Soler, 2004]
316L	450	100, 1500	6×10^{-8}	H_2/H_2O	9.7/0.035		Oxidation	Cr oxide	[Soler, 2004]
316L	600	100	1.1×10^{-8}	H_2/H_2O	9.7/0.035	20	Oxidation		[Soler, 2004]
316L	600	1500	1.1×10^{-8}	H_2/H_2O	9.7/0.035	-83	Dissolution		[Soler, 2004]
316L	450	500	1.1×10^{-8}	$Ar + H_2$	9.7/0.035		Oxidation	Cr oxidation	[Soler, 2004]
316L	450	2400	1.1×10^{-8}	$Ar + H_2$	9.7/0.035	-25	Dissolution	Slight dissolution	[Soler, 2004]
316L	600	500	1.1×10^{-8}	$Ar + H_2$	9.7/0.035	-40	Dissolution	Coexistence of dissolution and oxidation	[Soler, 2004]
316L	600	1500	1.1×10^{-8}	$Ar + H_2$	9.7/0.035	-63	Dissolution		[Soler, 2004]
316L	300	1500	1.85×10^{-5}	Saturation			Oxidation	Thin	[Long Bin, 2003]
316L	400	1500	1.41×10^{-4}	Saturation			Oxidation	Thin	[Long Bin, 2003]
316L	550	1500	1.17×10^{-3}	Saturation			Oxidation	Thin. Discontinuous and spongy.	[Long Bin, 2003]
316L	550	3000	1.17×10^{-3}	Saturation			Oxidation	Thin. Pb-Bi penetration.	[Long Bin, 2003]
316L	300	5000	1.85×10^{-5}	Saturation			Oxidation		[Long Bin, 2003]
316L	400	5000	1.41×10^{-4}	Saturation			Oxidation		[Long Bin, 2003]
316L	550	5000	1.17×10^{-3}	Saturation			Oxidation	Thin. Pb-bi penetration deeper	[Long Bin, 2003]
316L	500	800	1×10^{-6}	H_2/H_2O		6	Oxidation	Oxide nodes	[Müller, 2004]
316L	500	2000	1×10^{-6}	H_2/H_2O		6	Oxidation	Oxide nodes	[Müller, 2004]

Table 6.3.4. Fe-Cr-Ni steels in stagnant LBE (*cont.*)

Material	T (ºC)	Time (hours)	[O] (%wt.)	OCS	Surface sample/LBE volume ratio (cm^2/l)	Oxide thickness/ dissolution depth (microns)	Remark 1	Remark 2	Ref.
316L	500	5000	1×10^{-6}	H_2/H_2O		6	Oxidation	Oxide nodes	[Müller, 2004]
316L	500	10000	1×10^{-6}	H_2/H_2O		-40	Dissolution	Coexistence with oxide layers	[Müller, 2004]
316L	550	800	1×10^{-6}	H_2/H_2O		10-20	Oxidation	Air intake	[Müller, 2004]
316L	550	2000	1×10^{-6}	H_2/H_2O		10-20	Oxidation	Air intake	[Müller, 2004]
316L	550	5000	1×10^{-6}	H_2/H_2O		15	Oxidation	Pb-Bi penetration	[Müller, 2004]
316L	550	10000	1×10^{-6}	H_2/H_2O		-200	Dissolution		[Müller, 2004]
316L	600	800	1×10^{-6}	H_2/H_2O		-5-10	Dissolution	Thin spinel	[Müller, 2004]
316L	600	2000	1×10^{-6}	H_2/H_2O		-20	Dissolution		[Müller, 2004]
316L	600	5000	1×10^{-6}	H_2/H_2O		-20	Dissolution		[Müller, 2004]
316L	600	10000	1×10^{-6}	H_2/H_2O		-180	Dissolution		[Müller, 2004]
316L	450	550	3.14×10^{-4}			<3	Oxidation		[Gnecco, 2004]
316L*	550	550		Ar N60		7	Oxidation		[Gnecco, 2004]
316L*	600	550		Ar N60		20	Oxidation		[Gnecco, 2004]
316L*	350	1000		Ar N60		-	Oxidation		[Gnecco, 2004]
316L*	450	1000		Ar N60		3	Oxidation		[Gnecco, 2004]
316L	550	1000	1.17×10^{-3}			8	Oxidation		[Gnecco, 2004]
316L*	600	1000		Ar N60		<20	Oxidation		[Gnecco, 2004]
316L	550	550	3.9×10^{-9}	Ar + 5%H_2		-50	Dissolution		[Gnecco, 2004]
304L	550	100	4×10^{-7}	H_2/H_2O	5/0.004	-28	Dissolution		[Martín, 2004]
304L	535	3000	3×10^{-7}	H_2/H_2O	5/0.004		Oxidation	Cr oxide	[Martín, 2004]
304L	550	3000	4×10^{-7}	H_2/H_2O	5/0.004		Oxidation	Cr oxide	[Martín, 2004]
304L	535	500	8×10^{-6}	H_2/H_2O	5/0.004		Oxidation	Cr oxide	[Martín, 2004]
304L	550	500	8×10^{-6}	H_2/H_2O	5/0.004	11	Oxidation	Oxide nodules	[Martín, 2004]
304L	600	500	8×10^{-6}	H_2/H_2O	5/0.004	32	Oxidation	Oxide nodules	[Martín, 2004]
304L	535	3000	3×10^{-6}	H_2/H_2O	5/0.004	-35	Dissolution		[Martín, 2004]
304L	550	3000	4×10^{-6}	H_2/H_2O	5/0.004		Oxidation	Cr oxide	[Martín, 2004]
304L	600	3000	8×10^{-5}	H_2/H_2O	5/0.004	60	Oxidation	Oxide nodules	[Martín, 2004]
304L	450	3000	6×10^{-8}	H_2/H_2O	5/0.004		Oxidation	Cr oxide	[Gómez, 2004]
304L-preox	450	3000	6×10^{-8}	H_2/H_2O	5 /0.004		Oxidation	Cr oxide	[Gómez, 2004]
304L	600	100	4.7×10^{-4}	Ar + H_2 + H_2O	9.7/0.035	0.5	Oxidation		[Soler, 2004]
304L	600	500, 1500	4.7×10^{-4}	Ar + H_2 + H_2O	9.7/0.035	0.5	Oxidation	Oxide nodules 60	[Soler, 2004]

Table 6.3.4. Fe-Cr-Ni steels in stagnant LBE (*cont.*)

Material	T (ºC)	Time (hours)	[O] (%wt.)	OCS	Surface sample/LBE volume ratio (cm^2/l)	Oxide thickness/ dissolution depth (microns)	Remark 1	Remark 2	Ref.
304L	600	100	2×10^{-3}	Ar-saturation	9.7/0.035	0.2	Oxidation		[Soler, 2004]
304L	600	500	2×10^{-3}	Ar-saturation	9.7/0.035		Oxidation	Oxide nodules 17	[Soler, 2004]
304L	600	1500	2×10^{-3}	Ar-saturation	9.7/0.035			Slight dissolution	[Soler, 2004]
304L	450	500	3×10^{-4}	Ar-saturation	9.7/0.035		Oxidation	Cr oxide	[Soler, 2004]
304L	450	100, 1500	6×10^{-8}	H_2/H_2O	9.7/0.035		Oxidation	Cr oxide	[Soler, 2004]
304L	600	100	1.1×10^{-8}	H_2/H_2O	9.7/0.035		Oxidation	Cr oxide	[Soler, 2004]
304L	600	1500	1.1×10^{-8}	H_2/H_2O	9.7/0.035	-400	Dissolution		[Soler, 2004]
304L	450	500	1.1×10^{-8}	$Ar + H_2$	9.7/0.035		Oxidation	Cr oxidation	[Soler, 2004]
304L	450	2400	1.1×10^{-8}	$Ar + H_2$	9.7/0.035	-7	Dissolution	Slight dissolution	[Soler, 2004]
304L	600	500	1.1×10^{-8}	$Ar + H_2$	9.7/0.035		Dissolution	Slight dissolution	[Soler, 2004]
304L	600	1500	1.1×10^{-8}	$Ar + H_2$	9.7/0.035	-83	Dissolution		[Soler, 2004]
JPCA	450	3000	3.2×10^{-4}	Ar-saturation	21.6/0.7	2.76	Oxidation		[Kurata, 2005]
316ss	450	3000	3.2×10^{-4}	Ar-saturation	21.6/0.7	2.58	Oxidation		[Kurata, 2005]
SX	450	3000	3.2×10^{-4}	Ar-saturation	21.6/0.7	0.3	Oxidation		[Kurata, 2005]
JPCA	550	3000	1.2×10^{-3}	Ar-saturation	21.6/0.7	-43.6	Dissolution		[Kurata, 2005]
316ss	550	3000	1.2×10^{-3}	Ar-saturation	21.6/0.7	-22.41	Dissolution		[Kurata, 2005]
SX	550	3000	1.2×10^{-3}	Ar-saturation	21.6/0.7	0.48	Oxidation	SiO	[Kurata, 2005]

* Not clarified enough (oxygen content information missed).

Table 6.3.5. Fe-Cr steels in flowing LBE

Material	T (°C)	ΔT	Time (hours)	[O] (%wt.)	OCS	Loop	Volume LBE (l)	Flow rate (m/s)	Oxide thickness/ dissolution depth (microns)	Remark 1	Remark 2	Ref.
F82H	500	100	340, 1030	6×10^{-6}	Ar + 10 ppm	CIRCO	1.2	0.06	2.5-3.5	Oxidation	Exposure from beginning of operation	[Gómez, 2001]
F82H	500	100	3000	6×10^{-6}	Ar + 10 ppm	CIRCO	1.2	0.06	20	Oxidation	Exposure from beginning of operation	[Gómez, 2001]
F82H	500	100	690	6×10^{-6}	Ar + 10 ppm	CIRCO	1.2	0.06	-50	Dissolution	Intermediate time. Specimens inserted after 340 h from starting.	[Gómez, 2001]
F82H	500	100	960	6×10^{-6}	Ar + 10 ppm	CIRCO	1.2	0.06		Dissolution	Intermediate time. Specimens inserted after 1030 h from starting.	[Gómez, 2001]
F82H	500	100	1992	6×10^{-6}	Ar + 10 ppm	CIRCO	1.2	0.06	-140	Dissolution	Intermediate time. Specimens inserted after 1030 h from starting.	[Gómez, 2001]
F82H	500	100	1032	6×10^{-6}	Ar + 10 ppm	CIRCO	1.2	0.06	<1	Oxidation	Intermediate time. Specimens inserted after 1990 h from starting.	[Gómez, 2001]
F82H	550		1000	3.6×10^{-7}	H_2/H_2O = 0.12-2.2			2		Dissolution	Erosion damage	[Takahashi, 2002]
F82H	550	150	1000	2×10^{-9}	H_2/H_2O		22	2	-22	Dissolution	Severe erosion	[Kondo, 2005]
STBA28	550		1000	3.6×10^{-7}	H_2/H_2O = 0.12-2.2			2	-20	Dissolution		[Takahashi, 2002]
STBA28	550	150	1000	2×10^{-9}	H_2/H_2O		22	2	-20	Dissolution	No erosion	[Kondo, 2005]
T91	300	170	1116, 2000, 3116	$1\text{-}2 \times 10^{-6}$	He-20%H_2 PbO	Cu-1 M (IPPE) Preoxidated	60	2			Heterogeneous oxidation	[Barbier, 2001]
T91	470	170	1116	$1\text{-}2 \times 10^{-6}$	He-20%H_2 PbO	Cu-1 M (IPPE) Preoxidated	60	2	11	Oxidation	Weight gain (mg/mm^2): 0.35	[Barbier, 2001]
T91	470	170	2000	$1\text{-}2 \times 10^{-6}$	He-20%H_2 PbO	Cu-1 M (IPPE) Preoxidated	60	2	14	Oxidation	Weight gain (mg/mm^2): 0. 5	[Barbier, 2001]
T91	470	170	3116	$1\text{-}2 \times 10^{-6}$	He-20%H_2 PbO	Cu-1 M (IPPE) Preoxidated	60	2	16	Oxidation	Weight gain (mg/mm^2): 0.45	[Barbier, 2001]
T91	400		1500	3.1×10^{-10}-7.3×10^{-8}	Mg + Ar/H_2	LECOR	60	1		Dissolution	2.9×10^{-3} μm/h	[Fazio, 2003]

Table 6.3.5. Fe-Cr steels in flowing LBE (*cont.*)

Material	T (°C)	ΔT	Time (hours)	[O] (%wt.)	OCS	Loop	Volume LBE (l)	Flow rate (m/s)	Oxide thickness/ dissolution depth (microns)	Remark 1	Remark 2	Ref.
T91	400		1500	1×10^{-9}		LECOR		1	-1.97	Dissolution	Weight loss (mg/mm^2): 0.0375	[Aiello, 2004]
T91	400		4500	1×10^{-9}		LECOR		1	- 23.8	Dissolution	Weight loss (mg/mm^2): 0.184	[Aiello, 2004]
T91	400		1500	10^{-6}-10^{-5}		CHEOPE III		1	2-4	Oxidation	Weight gain(mg/mm^2): 3×10^{-4}	[Aiello, 2004]
T91	400		3000	10^{-6}-10^{-5}		CHEOPE III		1	6	Oxidation	Weight gain (mg/mm^2): 8.53×10^{-4}	[Aiello, 2004]
STBA26	550		959	5×10^{-7}	H_2/H_2O = 0.12-2.2			2			Weight loss (g/m^2): 16	[Takahashi, 2002]
STBA26	550		1000	3.6×10^{-7}	H_2/H_2O = 0.12-2.2			2	-20	Dissolution	Erosion damage	[Takahashi, 2002]
STBA26	550	150	1000	2×10^{-9}	H_2/H_2O		22	2	-16	Dissolution	Severe erosion	[Kondo, 2005]
Optifer IVc	300	170	1116	1-2 $\times 10^{-6}$	He-20%H_2 PbO	Cu-1M(IPPE) Preoxidated	60	2			Heterogeneous oxidation. Weight gain (mg/mm^2): 0.6.	[Barbier, 2001]
Optifer IVc	470	170	1116	1-2 $\times 10^{-6}$	He-20%H_2 PbO	Cu-1M (IPPE) Preoxidated	60	2	16	Oxidation		[Barbier, 2001]
Optifer IVc	300	170	2000, 3116	1-2 $\times 10^{-6}$	He-20%H_2 PbO	Cu-1M (IPPE) Preoxidated	60	2			Heterogeneous oxidation	[Barbier, 2001]
Optifer IVc	470	170	2000	1-2 $\times 10^{-6}$	He-20%H_2 PbO	Cu-1M (IPPE) Preoxidated	60	2	18	Oxidation	Weight gain(mg/mm^2): 0.7	[Barbier, 2001]
Optifer IVc	470	170	3116	1-2 $\times 10^{-6}$	He-20%H_2 PbO	Cu-1M (IPPE) Preoxidated	60	2	22	Oxidation		[Barbier, 2001]
Manet II	420	180	2000	1×10^{-6}		IPPE	60	1.3	10	Oxidation		[Müller, 2002]
Manet II	420	180	4000	1×10^{-6}	ArH_2 + PbO	IPPE	60	1.3	15	Oxidation		[Müller, 2004]
Manet II	550		2000	1×10^{-6}		Prometey	60	0.5	40	Oxidation		[Müller, 2002]
Manet II	550		4000	1×10^{-6}	ArH_2 + PbO		60			Oxidation	Spalls	[Müller, 2004]
Manet II	550		7200	1×10^{-6}	ArH_2 + PbO	Prometey		0.5	25	Oxidation	New oxide	[Müller, 2004]
ODS	550		1000	3.6×10^{-7}	H_2/H_2O = 0.12-2.2			2				[Takahashi, 2002]
ODS	550	150	1000	2×10^{-9}	H_2/H_2O		22	2	-5	Dissolution	No erosion	[Kondo, 2005]

Table 6.3.5. Fe-Cr steels in flowing LBE (*cont.*)

Material	T (°C)	ΔT	Time (hours)	[O] (%wt.)	OCS	Loop	Volume LBE (l)	Flow rate (m/s)	Oxide thickness/ dissolution depth (microns)	Remark 1	Remark 2	Ref.
EP823	300	170	1116, 2000, 3116	$1\text{-}2 \times 10^{-6}$	He-20%H_2 PbO	Cu-1M (IPPE) Preoxidated	60	2			Heterogeneous oxidation	[Barbier, 2001]
EP823	470	170	1116	$1\text{-}2 \times 10^{-6}$	He-20%H_2 PbO	Cu-1M (IPPE) Preoxidated	60	2	6	Oxidation	Weight gain (mg/mm^2): 0.25	[Barbier, 2001]
EP823	470	170	2000	$1\text{-}2 \times 10^{-6}$	He-20%H_2 PbO	Cu-1M (IPPE) Preoxidated	60	2	7.5	Oxidation	Weight gain (mg/mm^2): 0.25	[Barbier, 2001]
EP823	470	170	3116	$1\text{-}2 \times 10^{-6}$	He-20%H_2 PbO	Cu-1M (IPPE) Preoxidated	60	2	10	Oxidation	Weight gain (mg/mm^2): 0.25	[Barbier, 2001]
EP823	350		700	4×10^{-6}		CU-2- IPPE		2			Thin	[Benamati, 2002]
EP823	450		700	4×10^{-6}		CU-2 —IPPE		2	0.2-6.5			[Benamati, 2002]
EP823	550		700	4×10^{-6}		CU-2 —IPPE		2	0.6-11.5			[Benamati, 2002]
EP823 rod	460	300	1000	$3\text{-}5 \times 10^{-6}$		CU-1M-IPPE	60	1.9	0		Weight gain (mg/mm^2): 0.003	[Li, 2001]
EP823 rod	550	300	1000	$3\text{-}5 \times 10^{-6}$		CU-1M-IPPE	60	1.9	1		Weight loss (mg/mm^2): 0.001	[Li, 2001]
EP823 rod	460	300	2000	$3\text{-}5 \times 10^{-6}$		CU-1M-IPPE	60	1.9	7		Weight gain (mg/mm^2): 0.003	[Li, 2001]
EP823 rod	550	300	2000	$3\text{-}5 \times 10^{-6}$		CU-1M-IPPE	60	1.9	2		Weight gain(mg/mm^2): 0.001	[Li, 2001]
EP823 rod	460	300	3000	$3\text{-}5 \times 10^{-6}$		CU-1M-IPPE	60	1.9	6	Oxidation	Weight gain (mg/mm^2): 0.008	[Li, 2001]
EP823 rod	550	300	3000	$3\text{-}5 \times 10^{-6}$		CU-1M-IPPE	60	1.9	11	Oxidation	Weight gain (mg/mm^2): 0.00	[Li, 2001]
HT-9 tube	460	300	1000	$3\text{-}5 \times 10^{-6}$		CU-1M-IPPE	60	1.9	5		Weight gain(mg/mm^2): 0.002	[Li, 2001]
HT-9 tube	550	300	1000	$3\text{-}5 \times 10^{-6}$		CU-1M-IPPE	60	1.9	20		Weight gain (mg/mm^2): 0.003	[Li, 2001]
HT-9 tube	460	300	2000	$3\text{-}5 \times 10^{-6}$		CU-1M-IPPE	60	1.9	13		Weight gain(mg/mm2): 0.025	[Li, 2001]
HT-9 tube	550	300	2000	$3\text{-}5 \times 10^{-6}$		CU-1M-IPPE	60	1.9	34		Weight gain(mg/mm2): 0.04	[Li, 2001]
HT-9 tube	460	300	3000	$3\text{-}5 \times 10^{-6}$		CU-1M-IPPE	60	1.9	15	Oxidation	Weight gain (mg/mm2): 0.026	[Li, 2001]

Table 6.3.5. Fe-Cr steels in flowing LBE (*cont.*)

Material	T (°C)	ΔT	Time (hours)	[O] (%wt.)	OCS	Loop	Volume LBE (l)	Flow rate (m/s)	Oxide thickness/ dissolution depth (microns)	Remark 1	Remark 2	Ref.
HT-9 tube	550	300	3000	$3\text{-}5 \times 10^{-6}$		CU-1M-IPPE	60	1.9	25	Oxidation	Weight loss (mg/mm^2): 0.004	[Li, 2001]
SCM420	550		959	5×10^{-7}	H_2/H_2O = 0.12-2.2			2			Weight loss (g/m2): 38	[Takahashi, 2002]
SCM420	550		1000	3.6×10^{-7}	H_2/H_2O = 0.12-2.2			2	-40	Dissolution	Erosion damage	[Takahashi, 2002]
SCM420	550	150	1000	2×10^{-9}	H_2/H_2O		22	2	-40	Dissolution	Severe erosion	[Kondo, 2005]
SUS405	550		959	5×10^{-7}	H_2/H_2O = 0.12-2.2			2			Weight loss (g/m2): 11	[Takahashi, 2002]
SUS430	550		959	5×10^{-7}	H_2/H_2O = 0.12-2.2			2			Weight loss (g/m2): 9	[Takahashi, 2002]
NF616	550	150	1000	2×10^{-9}	H_2/H_2O		22	2	-15	Dissolution	No erosion	[Kondo, 2005]
NF616	550		1000	3.6×10^{-7}	H_2/H_2O = 0.12-2.2			2				[Takahashi, 2002]
HCM12	550	150	1000	2×10^{-9}	H_2/H_2O		22	2	-21	Dissolution	Crack-like erosion	[Kondo, 2005]
HCM12	550		1000	3.6×10^{-7}	H_2/H_2O = 0.12-2.2			2			Erosion damage (crack)	[Takahashi, 2002]
HCM12A	550	150	1000	2×10^{-9}	H_2/H_2O		22	2	-15	Dissolution	No erosion	[Kondo, 2005]
HCM12A	550		1000	3.6×10^{-7}	H_2/H_2O = 0.12-2.2			2				[Takahashi, 2002]
T-410 rod	460	300	1000	$3\text{-}5 \times 10^{-6}$		CU-1M-IPPE	60	1.9	6		Local corrosion more severe. No surface treatment.	[Li, 2001]
T-410 rod	550	300	1000	$3\text{-}5 \times 10^{-6}$		CU-1M-IPPE	60	1.9	15		Local corrosion more severe. No surface treatment.	[Li, 2001]
T-410 rod	460	300	2000	$3\text{-}5 \times 10^{-6}$		CU-1M-IPPE	60	1.9	13		Local corrosion more severe. No surface treatment.	[Li, 2001]
T-410 rod	550	300	2000	$3\text{-}5 \times 10^{-6}$		CU-1M-IPPE	60	1.9	24		Local corrosion more severe. No surface treatment.	[Li, 2001]

Table 6.3.5. Fe-Cr steels in flowing LBE (*cont.*)

Material	T (°C)	ΔT	Time (hours)	[O] (%wt.)	OCS	Loop	Volume LBE (l)	Flow rate (m/s)	Oxide thickness/ dissolution depth (microns)	Remark 1	Remark 2	Ref.
T-410 rod	460	300	3000	$3\text{-}5 \times 10^{-6}$		CU-1M-IPPE	60	1.9	13	Dissolution	Local corrosion more severe. No surface treatment.	[Li, 2001]
T-410 rod	550	300	3000	$3\text{-}5 \times 10^{-6}$		CU-1M-IPPE	60	1.9	19	Dissolution	Local corrosion more severe. No surface treatment.	[Li, 2001]

Table 6.3.6. Fe-Cr-Ni steels in flowing LBE

Material	T (°C)	ΔT	Time (hours)	[O] (%wt.)	OCS	Loop	LBE volume (litres)	Flow rate (m/s)	Oxide thickness/ dissolution depth (microns)	Remark 1	Remark 2	Ref.
D-9 tube	460	300	1000	$3\text{-}5 \times 10^{-6}$		CU-1M (IPPE)	60	1.9	0		Weight gain (mg/mm^2): 0.00	[Li, 2001]
D-9 tube	550	300	1000	$3\text{-}5 \times 10^{-6}$		CU-1M (IPPE)	60	1.9	12		Weight gain (mg/mm^2): 0.009	[Li, 2001]
D-9 tube	460	300	2000	$3\text{-}5 \times 10^{-6}$		CU-1M (IPPE)	60	1.9	5		Weight gain (mg/mm^2): 0.002	[Li, 2001]
D-9 tube	550	300	2000	$3\text{-}5 \times 10^{-6}$		CU-1M (IPPE)	60	1.9	26		Weight gain (mg/mm^2): 0.013	[Li, 2001]
D-9 tube	460	300	3000	$3\text{-}5 \times 10^{-6}$		CU-1M (IPPE)	60	1.9	4		Weight gain (mg/mm^2): 0.006	[Li, 2001]
D-9 tube	550	300	3000	$3\text{-}5 \times 10^{-6}$		CU-1M (IPPE)	60	1.9	24		Weight gain (mg/mm^2): 0.002	[Li, 2001]
1.4970	300	170	1116, 2000	$1\text{-}2 \times 10^{-6}$	He-20%H_2 PbO	Cu-1M(IPPE) Preoxidated	60	2				[Barbier, 2001]
1.4970	470	170	1116	$1\text{-}2 \times 10^{-6}$	He-20%H_2 PbO	Cu-1M (IPPE) Preoxidated	60	2			Weight gain: 0.01	[Barbier, 2001]
1.4970	470	170	2000	$1\text{-}2 \times 10^{-6}$	He-20%H_2 PbO	Cu-1M (IPPE) Preoxidated	60	2			Weight gain: 0.04	[Barbier, 2001]
1.4970	300	170	3116	$1\text{-}2 \times 10^{-6}$	He-20%H_2 PbO	Cu-1M (IPPE) Preoxidated	60	2	<1	Oxidation		[Barbier, 2001]
1.4970	470	170	3116	$1\text{-}2 \times 10^{-6}$	He-20%H_2 PbO	Cu-1M (IPPE) Preoxidated	60	2	<1	Oxidation	Weight gain: 0.02	[Barbier, 2001]
1.4970	420	180	2000, 4000	1×10^{-6}		IPPE	60	1.3	<1			[Müller, 2002]
1.4970	550		2000	1×10^{-6}		Prometey	60	0.5	30		Nodules	[Müller, 2002]
1.4970	550		4300	1×10^{-6}	ArH_2 + PbO	Prometey	60	0.5	15		Pb-Bi infiltration	[Müller, 2004]
1.4970	550		7200	1×10^{-6}	ArH_2 + PbO	Prometey	60	0.5	15 + 15		No LBE infiltration and growing of new oxide layer underneath	[Müller, 2004]
1.4970	600	180	2000	1×10^{-6}		IPPE	60	1.3	30		Nodules	[Müller, 2002]
1.4970	600	180	4000	1×10^{-6}	ArH_2 + PbO	IPPE	60	1.3	-100	Dissolution		[Müller, 2004]
316L	420	180	2000, 4000	1×10^{-6}		IPPE	60	1.3	<1	Oxidation		[Müller, 2002]
316L	550		2000	1×10^{-6}		Prometey	60	0.5		Oxidation	Nodules	[Müller, 2002]

Table 6.3.6. Fe-Cr-Ni steels in flowing LBE (*cont.*)

Material	T (°C)	ΔT	Time (hours)	[O] (%wt.)	OCS	Loop	LBE volume (litres)	Flow rate (m/s)	Oxide thickness/ dissolution depth (microns)	Remark 1	Remark 2	Ref.
316L	550		4000	1×10^{-6}	ArH_2 + PbO	Prometey	60	0.5	15	Oxidation	Gap between spinel and magnetite	[Müller, 2004]
316L	550		7200	1×10^{-6}		Prometey	60	0.5	5	Oxidation	New oxide layer	[Müller, 2004]
316L	600	180	2000	1×10^{-6}		IPPE	60	1.3	-200	Dissolution		[Müller, 2002]
316L	400		1500	3.1×10^{-10}-7.3×10^{-8}	Mg +Ar/H_2	LECOR	60	1		Dissolution	1.9×10^{-3} μm/h	[Fazio, 2003]
316L	550	150	1000	2×10^{-9}	H_2/H_2O		22.	2	-100	Dissolution	Erosion started	[Kondo, 2005]
316L-tube	460	300	1000	3-5 $\times 10^{-6}$		CU-1M (IPPE)	60	1.9	0		Weight gain(mg/mm^2): 0.00	[Li, 2001]
316L-tube	550	300	1000	3-5 $\times 10^{-6}$		CU-1M (IPPE)	60	1.9	7		Weight loss (mg/mm^2): 0.001	[Li, 2001]
316 tube	460	300	2000	3-5 $\times 10^{-6}$		CU-1M (IPPE)	60	1.9	3		Weight loss (mg/mm^2): 0.002	[Li, 2001]
316L-tube	550	300	2000	3-5 $\times 10^{-6}$		CU-1M (IPPE)	60	1.9	18		Weight gain(mg/mm^2): 0.019	[Li, 2001]
316 tube	460	300	3000	3-5 $\times 10^{-6}$		CU-1M (IPPE)	60	1.9	4		Weight gain (mg/mm^2): 0.00	[Li, 2001]
316L-tube	550	300	3000	3-5 $\times 10^{-6}$		CU-1M (IPPE)	60	1.9	21		Weight gain(mg/mm^2): 0.00	[Li, 2001]
316L rod	460	300	1000	3-5 $\times 10^{-6}$		CU-1M (IPPE)	60	1.9	0		Local corrosion No surface treat. Weight gain (mg/mm^2) 0.002.	[Li, 2001]
316L rod	550	300	1000	3-5 $\times 10^{-6}$		CU-1M (IPPE)	60	1.9	1		Local corrosion No surface treat. Weight gain (mg/mm^2) 0.01.	[Li, 2001]
316L rod	460	300	2000	3-5 $\times 10^{-6}$		CU-1M (IPPE)	60	1.9	0		Local corrosion No surface treat. Weight loss (mg/mm^2): 0.002.	[Li, 2001]
316L rod	550	300	2000	3-5 $\times 10^{-6}$		CU-1M (IPPE)	60	1.9	2		Local corrosion No surface treat. Weight gain (mg/mm^2) 0.00.	[Li, 2001]
316L rod	460	300	3000	3-5 $\times 10^{-6}$		CU-1M (IPPE)	60	1.9	0		Local corrosion No surface treat.Weight gain (mg/mm^2): 0.000.	[Li, 2001]

Table 6.3.6. Fe-Cr-Ni steels in flowing LBE (*cont.*)

Material	T (°C)	ΔT	Time (hours)	[O] (%wt.)	OCS	Loop	LBE volume (litres)	Flow rate (m/s)	Oxide thickness/ dissolution depth (microns)	Remark 1	Remark 2	Ref.
316L rod	550	300	3000	$3\text{-}5 \times 10^{-6}$		CU-1M (IPPE)	60	1.9	2		Local corrosion No surface treat. Weight loss (mg/mm^2): 0.02.	[Li, 2001]
SS316	550		959	5×10^{-7}	H_2/H_2O = 0.12-2.2			2	30	Oxidation	Porous layer. Weight loss (g/m^2): 62.	[Takahashi, 2002]
SS316	550		1000	3.6×10^{-7}	H_2/H_2O = 0.12-2.2			2	-100	Dissolution		[Takahashi, 2002]
316L	400		1500	1×10^{-9}		LECOR		1	-0.64	Dissolution	Weight loss (mg/mm^2): 0.0225	[Aiello, 2004]
316L	400		4500	1×10^{-9}		LECOR		1	-19.5	Dissolution	Weight loss (mg/mm^2): 0.155	[Aiello, 2004]
316L	400		1500	10^{-6}-10^{-5}		CHEOPE III		1	1	Oxidation	Weight gain (mg/mm^2): 2.9×10^{-3}	[Aiello, 2004]
316L	400		3000	10^{-6}-10^{-5}		CHEOPE III		1		Oxidation	Weight gain (mg/mm^2): 3.91×10^{-3}	[Aiello, 2004]

Table 6.3.7. Steels in stagnant Pb

Material	T (ºC)	Time (hours)	[O] (%wt.)	OCS	Surface sample/ LBE volume ratio	Oxide thickness/ dissolution depth (microns)	Remark 1	Remark 2	Ref.
Optifer IVc	550	800	8×10^{-6}	H_2/H_2O					[Müller, 2000]
Optifer IVc	550	1500	8×10^{-6}	H_2/H_2O					[Müller, 2000]
Optifer IVc	550	3000	8×10^{-6}	H_2/H_2O		35	Oxidation		[Müller, 2000]
1.4970	550	800	8×10^{-6}	H_2/H_2O					[Müller, 2000]
1.4970	550	1500	8×10^{-6}	H_2/H_2O					[Müller, 2000]
1.4970	550	3000	8×10^{-6}	H_2/H_2O		16	Oxidation	Pb inclusions at the oxide/ material interface	[Müller, 2000]
F82H	464	700		Argon		8	Oxidation		[Fazio, 2001]
F82H	464	1200		Argon		20	Oxidation		[Fazio, 2001]
316L	464	700		Argon			Oxidation	Not measurable	[Fazio, 2001]
316L	464	1200		Argon		2-4	Oxidation		[Fazio, 2001]
F82H	520	2000		Argon (saturation)	$13.7 cm^2/0.3$ l	20	Oxidation	Weight gain: 0.0741	[Benamati, 2000]
F82H	520	3700		Argon (saturation)	$13.7 cm^2/0.3$ l	40	Oxidation	Weight gain: 0.1652	[Benamati, 2000]

Table 6.3.8. Steels in flowing Pb

Material	T (°C)	ΔT	Time (hours)	[O] (%wt.)	OCS	Loop	LBE volume (l)	Flow rate (m/s)	Oxide thickness/ dissolution depth (microns)	Remark 1	Ref.
Optifer Ivc	400		1027	$3\text{-}4 \times 10^{-5}$		IPPE	60	2	36	Oxidation	[Glasbrenner, 2001]
Optifer Ivc	550		1027	$3\text{-}4 \times 10^{-5}$		IPPE	60	2			[Glasbrenner, 2001]
Optifer Ivc	400		200	$3\text{-}4 \times 10^{-5}$		IPPE	60	2	44	Oxidation	[Glasbrenner, 2001]
Optifer Ivc	550		2000	$3\text{-}4 \times 10^{-5}$		IPPE	60	2			[Glasbrenner, 2001]
Optifer Ivc	400		3027	$3\text{-}4 \times 10^{-5}$		IPPE	60	2	49	Oxidation	[Glasbrenner, 2001]
Optifer Ivc	550		3027	$3\text{-}4 \times 10^{-5}$		IPPE	60	2	25	Oxidation	[Glasbrenner, 2001]
EM10	550		1027	$3\text{-}4 \times 10^{-5}$		IPPE	60	2	34	Oxidation	[Glasbrenner, 2001]
EM10	550		3027	$3\text{-}4 \times 10^{-5}$		IPPE	60	2			[Glasbrenner, 2001]
1.4948	400		1027	$3\text{-}4 \times 10^{-5}$		IPPE	60	2	2	Oxidation	[Glasbrenner, 2001]
1.4948	550		1027	$3\text{-}4 \times 10^{-5}$		IPPE	60	2			[Glasbrenner, 2001]
1.4948	400		2000	$3\text{-}4 \times 10^{-5}$		IPPE	60	2	2	Oxidation	[Glasbrenner, 2001]
1.4948	550		2000	$3\text{-}4 \times 10^{-5}$		IPPE	60	2			[Glasbrenner, 2001]
1.4948	400		3027	$3\text{-}4 \times 10^{-5}$		IPPE	60	2			[Glasbrenner, 2001]
1.4948	550		3027	$3\text{-}4 \times 10^{-5}$		IPPE	60	2	2	Oxidation	[Glasbrenner, 2001]
1.4970	400		1027	$3\text{-}4 \times 10^{-5}$		IPPE	60	2			[Glasbrenner, 2001]
1.4970	550		1027	$3\text{-}4 \times 10^{-5}$		IPPE	60	2	2	Oxidation	[Glasbrenner, 2001]
1.4970	400		2000	$3\text{-}4 \times 10^{-5}$		IPPE	60	2			[Glasbrenner, 2001]
1.4970	550		2000	$3\text{-}4 \times 10^{-5}$		IPPE	60	2	2	Oxidation	[Glasbrenner, 2001]
1.4970	400		3027	$3\text{-}4 \times 10^{-5}$		IPPE	60	2			[Glasbrenner, 2001]
1.4970	550		3027	$3\text{-}4 \times 10^{-5}$		IPPE	60	2	2	Oxidation	[Glasbrenner, 2001]

REFERENCES

Aiello, A., M. Azzati, G. Benamati, A. Gessi, B. Long, G. Scaddozzo, (2004), "Corrosion Behaviour of Stainless Steels in Flowing LBE at Low and High Oxygen Concentration", *Journal of Nuclear Materials,* 335, pp. 169-173.

Bagnall, C, P.F. Tortorelli, J.H. DeVan, S.L. Schrock (1995), "Liquid Metals, Corrosion Tests and Standards", p. 387, edited by R. Baboian.

Balbaud-Celerier, F., A. Terlain, P. Fauvet, C. Richet (2003), *Corrosion of Steels in Liquid Lead Alloys Protected by an Oxide Layer Application to the MEGAPIE Target and to the Russian Reactor Concept BREST 300,* Report Technique RT-SCCME 630, CEA Report.

Barbier, F., A. Rusanov (2001), "Corrosion Behavior of Steels in Flowing Lead-bismuth", *Journal of Nuclear Materials*, 296, p. 23.

Benamati, G., P. Buttol, V. Imbeni, C. Martini, G. Palombarini (2000), "Behaviour of Materials for Accelerator Driven Systems in Stagnant Molten Lead", *Journal of Nuclear Materials*, 279, p.308.

Benamati, G., C. Fazio, H. Piankova, A. Rusanov (2002), "Temperature Effect on the Corrosion Mechanism of Austenitic and Martensitic Steels in Lead-bismuth", *Journal of Nuclear Materials*, 301, p. 23.

Chang, S.L., F.S. Pettit, N. Birks (1990), *Oxidation of Metals,* 34, 71.

Deloffre, Ph., A. Terlain, F. Barbier (2002), "Corrosion and Deposition of Ferrous Alloys in Molten Lead-bismuth", *Journal of Nuclear materials*, 301, p. 35.

Efanov, D., Yu.I. Orlov, P.N. Martynov, V.A. Gylevsky (2001), "Study of Lead Coolant Technology", 001 ANS Winter Meeting, Reno, Nevada, 11-15 November.

Fazio, C., G. Benamati, C. Martini, G. Palombarini (2001), "Compatibility Tests on Steels in Molten Lead and Lead-bismuth", *Journal of Nuclear Materials*, 296, p. 243.

Fazio, C., I. Ricapito, G. Scaddozzo, G. Benamati (2003), "Corrosion Behaviour of Steels and Refracto Metals and Tensile Features of Steels Exposed to Flowing PbBi in the LECOR Loop", *Journal of Nuclear Materials*, 318, p. 325.

Furukawa, J. (2004), *Nuclear Science and Technology*, 41, 3, 265.

Furukawa, T., G. Müller, G. Schumacher, A. Weisenburger, A. Heinzel, K. Aoto (2004), "Effect of Oxygen Concentration and Temperature on Compatibility of ODS Steel with Liquid, Stagnant $Pb_{45}Bi_{55}$", *Journal of Nuclear Materials,* 335, pp. 189-193.

Gerasimov, V., A. Monakhov (1983), *Nuclear Engineering Materials*, MIR1983.

Glasbrenner, H., J. Konys, G. Müller, A. Rusanov (2001), "Corrosion Investigation of Steels in Flowing Lead at 400°C and 550°C", *Journal of Nuclear Materials*, 296, p. 237.

Gnecco, F., E. Ricci, C. Bottino, A. Passerone (2004), "Corrosion Behaviour of Steels in Lead-bismuth at 823 K", *Journal of Nuclear Materials*, 335, pp. 185-188.

Gómez Briceño, D., F.J. Martín Muñoz, L. Soler Crespo, F. Esteban, C. Torres (2001), "Behaviour of F82Hmod. Stainless Steel in Lead-bismuth Under Temperature Gradient", J*ournal of Nuclear Materials*, 296, p. 265.

Gómez Briceño, D., L. Soler Crespo, F.J. Martín Muñoz, F. Hernández Arroyo (2002), "Influence of Temperature on the Oxidation/Corrosion Process of F82Hmod. Martensitic Steel in Lead-bismuth", *Journal of Nuclear Materials*, 303, p. 137.

Gómez Briceño, D., L. Soler Crespo, F.J. Martín Muñoz, F. Hernández (2004), *Oxide Formation Efficiency in Stagnant Lead-bismuth*, TECLA report, Deliverable 8.

Gorynin, V., G.P. Karzov, V.G. Markov V.A. Yakovlev (1999), "Structural Materials for Atomic Reactors with Liquid Metal Heat-transfer Agents in the Form of Lead or Lead-bismuth Alloy", *Metal Science and Heat Treatment*, Vol. 41, Nº 9-10, pp. 384-388.

Gorynin, V., G.P. Karzov, V.G. Markov, V.S. Lavrukhin V.A. Yakovlev (1998), "Structural Materials for Power Plants with Heavy Liquid Metals as Coolants", *Proceedings of the Conference Heavy Liquid Metals Coolants in Nuclear Technologie (HCLM-98)*, Volume 1, p. 120, Obninsk.

Gromov, B.F., G.I. Toshinky, *et al*. (1998), "Designing the Reactor Installation with Lead-bismuth Coolant for Nuclear Submarines. The Brief History. Summarised Operations Results", *Proceedings of the Conference Heavy Liquid Metals Coolants in Nuclear Technologies (HCLM-98)*, Volume 1, p. 14, Obninsk.

Gullevsky, V.A., P.N. Martynov, Yu.I. Orlov, M.E. Chernov (1998), "Application of Hydrogen/Water Vapor Mixtures in Heavy Coolant Technology", *Proceedings of the Conference Heavy Liquid Metals Coolants in Nuclear Technologies (HCLM-98)*, Volume 2, p. 668, Obninsk.

Knebel, J.U., G. Müller, G. Schumacher (1999), "Gas-phase Oxygen Control Processes for Lead/Bismuth Loops and Accelerator-driven Systems (ADS)", *Jahrestagung Kerntechnik*.

Kofstad, P. (1987), "High Temperature Corrosion", Elsevier Applied Science Publishers, Ltd, p. 413.

Kondo, M., M. Takahashi, T. Suzuki, K. Ishikawa, K. Hata, S. Qiu, H. Sekimoto (2005), "Metallurgical Study on Erosion and Corrosion Behaviors of Steels Exposed to Liquid Lead-bismuth Flow", *Journal of Nuclear Materials*, Vol. 343, pp. 349-359.

Kurata, Y., M. Futakawa, S. Saito (2005), "Comparison of the Corrosion Behavior of Austenitic and Ferritic/Martensitic Steels Exposed to Static Liquid Pb-Bi at 450 and 550°C", *Journal of Nuclear Materials*, 343, pp. 335-340.

Kurata, Y., M. Futakawa, K. Kikuchi, S. Saito, T. Osugi (2002), "Corrosion Studies in Liquid Pb-Bi Alloy at JAERI: R&D Program and First Experimental Results", *Journal of Nuclear Materials*, 301, p. 28.

Li, N. (2002), "Active Control of Oxygen in Molten Lead-bismuth Eutectic System to Prevent Steel Corrosion and Coolant Contamination", *Journal of Nuclear Materials*, Vol. 300, pp. 73-81.

Li, N., X. He, A. Rusanov, A.P. Demishonkov (2001), *Corrosion Tests of US Steels in Lead-bismuth Eutectic (LBE) and Kinetic Modelling of Corrosion in LBE Systems*, LA-UR-01-5241.

Long Bin (2003), IWMHR, Rome.

Martín, F.J., L. Soler, F. Hernández, D. Gómez-Briceño (2004), "Oxide Layer Stability in Lead-bismuth at High Temperature", *Journal of Nuclear Materials*, 335, pp. 194-198.

Martinelli, L., F. Balbaud-Celerier, S. Bosonnet, A. Terlain, G. Santarini, S. Delpech, G. Picard (2005), "High Temperature Oxidation of Fe-9Cr Steel in Stagnant Liquid Lead-bismuth", *Eurocorr2005*, Lisbon.

Müller, G., A. Heinzel, J. Konys, G. Schumacher, A. Weisenburger, F. Zimmermann, V. Engelko, A. Rusanov, V. Markov (2002), "Results of Steel Corrosion Tests in Flowing Liquid Pb/Bi at 420-600°C After 2000 h", *Journal of Nuclear Materials*, 301, p. 40.

Müller, G., A. Heinzel, J. Konys, G. Schumacher, A. Weisenburger, F. Zimmermann, V. Engelko, A. Rusanov, V. Markov (2004), "Behavior of Steels in Flowing Liquid PbBi Eutectic Alloy at 420-600°C After 4000-7200 h", *Journal of Nuclear Materials*, 335, p. 163.

Müller, G., A. Heinzel, G. Schumacher, A. Weisenburger (2003), "Control of Oxygen Concentration in Liquid Lead and Lead-bismuth", *Journal of Nuclear Materials*, Vol. 321, p. 256.

Müller, G., A. Heinzel, G. Schumacher, A. Weisenburger, F. Zimmermann (2004), *Protection by Restructuring and Alloying Surface Layer by Pulsed Electron Beam Facility*, TECLA report, Deliverable 11.

Müller, G., G. Schumacher, F. Zimmermann (2000), "Investigation on Oxygen Controlled Liquid Lead Corrosion of Surface Treated Steels", *Journal of Nuclear Materials*, 278, p. 85.

Rishel, D.M., F.S. Pettit, N. Birks (1991), *Materials Science and Engineering* A, 143, 197.

Shamatko, B.A., A. Rusanov (2000), "Oxide Protection of Materials in Melts of Lead and Bismuth", *Materials Science*, Vol. 36, No. 5, pp. 689-700.

Sheir, LL., R.A. Jarman, G.T. Burstein (eds.) (1994), "Metal/Environment Reactions", *Corrosion*, Chapter 2.9.

Soler Crespo, L., F.J. Martín Muñoz, D. Gómez Briceño (2001), "Short-term Static Corrosion Tests in Lead-bismuth, *Journal of Nuclear Materials*, 296, p. 273.

Soler, L., F.J. Martín, F. Hernández, D. Gómez-Briceño (2004), "Corrosion of Stainless Steels in Lead-bismuth Eutectic up to 600°C", *Journal of Nuclear Materials*, 335, pp. 174-179.

Staudhammer, P.K. (1992), *Materials Compatibility and Corrosion Issues for Accelerator Transmutation of Waste*, LA- 1227-MS.

Stott, F.H. (1987), *Rep. Prog. Phys*., 50, 861.

Takahashi, *INCONE 10* (2002).

Tortorelli, P.F., *et al*. (1987), "Metals Handbook", *Corrosion*, 9th Edition, Vol. 13.

Weeks, J.R. (1997), "Compatibility of Structural Materials with Liquid Lead-bismuth and Mercury", *Proceedings of the Symposium on Materials for Spallation Neutron Sources*, Orlando.

Yachmenyov, G.S., A.Ye. Rusanov, *et al*. (1998), "Problems of Structural Materials' Corrosion in Lead-bismuth Coolant. The Problem of Technology of the Heavy Liquid Metal Coolants (Lead, Lead-bismuth)", *HLMC-98*, pp. 133.

Zhang J., N. Li, J.S. Elson, *Progress in Materials Science* (forthcoming, 2004).